An Exceptionally Aqueous Stable Diruthenium *N*-Indolyl Aminocarbyne Complex as Prospective Anticancer Agent

Matteo Fiaschi,[a] Ján Vančo,[b] Lorenzo Biancalana,[a,*] Tomáš Malina,[b] Zdeněk Dvořák,[c] Tiziana Funaioli,[a] Stefano Zacchini,[d] Massimo Guelfi,[a] Zdeněk Trávníček,[b,*] and Fabio Marchetti[a,*]

[b] *University of Pisa, Department of Chemistry and Industrial Chemistry, Via G. Moruzzi 13, I-56124 Pisa, Italy.*

[a] *Regional Centre of Advanced Technologies and Materials, Czech Advanced Technology and Research Institute, Palacký University, Šlechtitelů 27, CZ-779 00 Olomouc, Czech Republic.*

[c] *Department of Cell Biology and Genetics, Faculty of Science, Palacký University, Šlechtitelů 27, CZ-779 00 Olomouc, Czech Republic.*

[d] *University of Bologna, Department of Industrial Chemistry "Toso Montanari", Viale del Risorgimento 4, I-40136 Bologna, Italy.*

* Email addresses: lorenzo.biancalana@unipi.it; zdenek.travnicek@upol.cz; fabio.marchetti@unipi.it.

Abstract

We conducted a systematic study on the reactivity of $[Ru_2Cp_2(CO)_4]$ (Cp = η^5-C_5H_5) with isocyanides and the subsequent methylation reaction to produce $[Ru_2Cp_2(CO)_2(\mu\text{-}CO)\{\mu\text{-}CNMe(R)\}]^+$ complexes as $CF_3SO_3^-$ salts, [**2a-h**]$^+$ [R = Me, cyclohexyl (Cy), 2,6-$C_6H_3Me_2$ (Xyl), 1*H*-indol-5-yl, 2-naphthyl, 4-C_6H_4OMe, (*S*)-CHMe(Ph), CH_2Ph (Bn)]. The resulting products, including five novel ones, underwent structural characterization by IR and multinuclear NMR spectroscopy, with five of them further confirmed via single crystal X-ray diffraction. Compounds [**2a-e,h**]CF_3SO_3 exhibit appreciable water

solubility, substantial amphiphilic character and outstanding stability in physiological-like solutions (negligible degradation after 72 hours in DMEM cell culture medium at 37 °C). Representative complexes [**2b**]$^+$ and [**2c**]$^+$ were additionally characterized through cyclic voltammetry in CH_2Cl_2 and in aqueous phosphate buffer solution.

Compounds [**2a-d**]CF_3SO_3 were assessed for *in vitro* cytotoxicity against A2780, A2080R and MCF-7 human cancer cell lines, and [**2a-c**]CF_3SO_3 revealed significant-to-moderate cytotoxicity, outperforming cisplatin in several cases. The most favorable IC_{50} values were observed for [**2d**]CF_3SO_3, ranging from 3.7 to 13.0 μM. Experiments on the noncancerous human cell line MRC-5 highlighted a reasonable selectivity for [**2b-d**]CF_3SO_3, with the highest selectivity indexes (SI) calculated as 10.1 (ratio of IC_{50} on MRC-5/ IC_{50} on A2780) and 8.5 (ratio of IC_{50} on MRC-5/ IC_{50} on A2780R) for [**2d**]CF_3SO_3. Subsequently, [**2d**]CF_3SO_3 was tested across a panel of HOS, A549, PANC1, CaCo2, PC3 and HeLa cancer cells, showing variable cytotoxicity with IC_{50} values in the range of 9.7 to 20.3 μM. The cellular effects of [**2d**]$^+$ on A2780 cells were investigated using flow cytometry assays, focusing on the cell cycle modification, time-resolved cellular uptake, intracellular ROS production, mitochondrial membrane depolarization, induction of cell death through apoptosis, activation of caspases 3/7 and induction of autophagy. Overall, the results suggest a diphasic mechanism of action for [**2d**]$^+$, inducing metabolic stress and arresting proliferation in the first/fast phase, followed by the induction of apoptosis and autophagy in the second/slower phase.

Keywords: metallodrugs; diruthenium complexes; aminocarbyne ligand; cellular effects; cytotoxicity; flow cytometry.

1. Introduction

Organometallic complexes based on transition elements offer an array of properties of potential usefulness for medicinal applications.[1,2,3,4] These include the availability of various geometries and metal oxidation states, the possibility of tuning physicochemical properties by modifying the ligands, and the potential to function as pro-drugs that can be activated upon reaching the desired biological target.[5] Indeed, a considerable variety of transition metal complexes with hydrocarbyl (C_xH_y) ligands have been proposed for pharmaceutical development.[1-5] Notable examples comprise ferroquine, a ferrocene derivative that has advanced to clinical trials as antimalarial drug,[6,7] and several ruthenium η^6-arene complexes, that have been extensively studied as promising anticancer agents.[8,9] Ruthenium species are regarded as relatively nontoxic and tolerated by the human body;[10,11] certain organo-ruthenium compounds exhibit potent antitumor potential in vivo, thus warranting consideration for clinical trials.[12,13] Some crucial pre-requisites are essential for the successful development of a metal-based drug, including straightforward synthesis, sufficient water solubility for administration, and a substantial inertness in physiological solutions.[14,15] Concerning the latter point, ligand dissociation (or ligand rearrangement) may serve as a preliminary functional step to favor the successive interaction of the metal centre with the biological target(s).[16,17] Notwithstanding, this process could ultimately lead to an undefined speciation and, potentially, undesired side effects.[18,19] In fact, a significant number of proposed anticancer ruthenium complexes undergo either rapid or progressive disruption of the coordination sphere in aqueous solutions.[20,21]

There are some substantial reasons that make the shifting to dimetallic systems a promising advancement in metal medicinal chemistry. Indeed, dimetallic systems provide an increased number of coordination sites, and the cooperative effects arising from two adjacent metal centres may enable unique reactivity patterns otherwise unattainable (*just as one hand is sufficient to eat an apple, but two hands are required to peel it*).[22,23,24,25,26] Together, these features enhance structural variability and diversity, allowing for the fine tuning of physicochemical properties.[27]

Recently, we have elucidated the biological properties of diiron complexes with a bridging aminocarbyne ligand, that can be synthesized from the commercial iron(I) dimer $[Fe_2Cp_2(CO)_4]$ ($Cp = \eta^5$-C_5H_5) through a broad-scope two-step procedure (Scheme 1).[28,29] The cytotoxicity of [**2a-j**^{Fe}]CF_3SO_3 is strictly dependent on the nature of the R substituent. Among this series, the most potent compounds, [**2b,f**^{Fe}]$^+$, demonstrated superior activity in challenging 3D cancer cell models, surpassing the efficacy of the benchmark drug *cisplatin*, and a noticeable inclination to selectivity compared to noncancerous cell lines.[30,31] The mechanism of action of diiron aminocarbyne complexes appears to be prevalently associated with the disruption of intracellular redox homeostasis,[31] triggered by the disassembly of the organo-diiron structure.

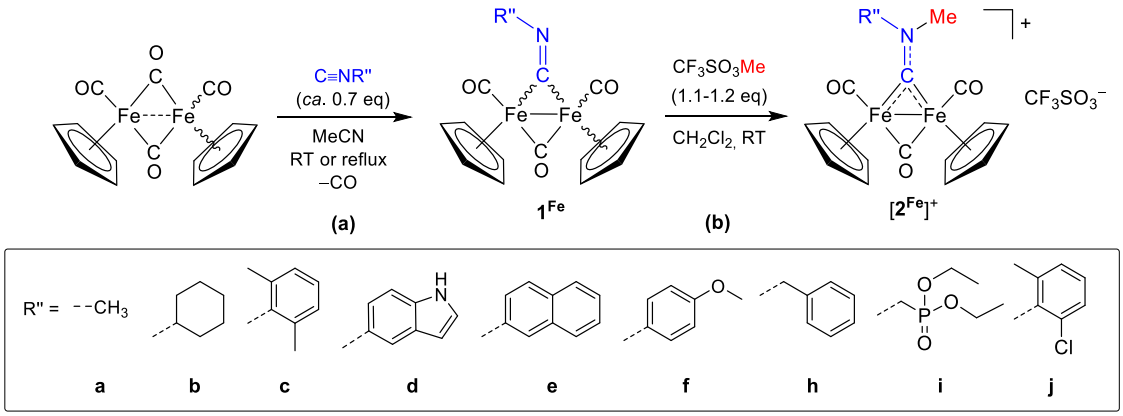

Scheme 1. Preparation of diiron bis-cyclopentadienyl isocyanide complexes by CO/CNR substitution on $[Fe_2Cp_2(CO)_4]$ (**a**)[32] and subsequent *N*-alkylation (methylation) affording μ-aminocarbyne complexes (**b**). Only one form of the fluxional complexes $[Fe_2Cp_2(CO)_3(CE)]$, E = O, NR, is depicted for simplicity.

We redirected our focus towards developing a similar biochemistry from the commercially available $[Ru_2Cp_2(CO)_4]$, which has not been explored hitherto. Note that the "diruthenium approach" has garnered increasing attention in medicinal chemistry,[33,34,35,36,37,38,39,40] nevertheless investigations on the anticancer potential of compounds with a Ru-Ru bonded core remain quite limited. In contributing to this field, we have recently unveiled the activity of $[Ru_2Cp_2(CO)_4]$ derivatives containing bridging allenyl[41] and vinyl ligands.[42]

In principle, the pathway illustrated in Scheme 1 can be extended to the homologous diruthenium compounds. However, there is limited information in the literature regarding the preparation of $[Ru_2Cp_2(CO)_3(CNR)]$, **1**, and $[Ru_2Cp_2(CO)_2(\mu\text{-}CO)\{\mu\text{-}CN(Me)R\}]^+$, $[\mathbf{2}]^+$ (Scheme 2). In fact, these systems were sparsely investigated in the 1980s and 1990s within the realm of pioneering organometallic chemistry, they were handled under inert atmosphere and no applicative studies were attempted. Specifically, $[Ru_2Cp_2(CO)_4]$ is known to react slowly with some alkyl isocyanides in refluxing xylene (boiling point ≈ 140 °C) to afford mono-substituted derivatives **1**, which were isolated by alumina chromatography (with yields unspecified).[43] Some unreacted $[Ru_2Cp_2(CO)_4]$ was recovered, indicating a partial conversion even in the presence of excess isocyanide. Under analogous conditions, $[Ru_2(Cp)_2(CO)_2(CNBn)]$ (**1h**)[44] was obtained in < 10 % yield. Instead, the reaction of $[Ru_2Cp_2(CO)_4]$ with excess benzyl or xylyl isocyanide and Me_3NO led to a mixture of mono- and di-substituted complexes $[Ru_2Cp_2(CO)_{3-x}(CNR)_x]$ (x = 1,2) which were isolated in modest yield through alumina chromatography. Methylation of the benzyl isocyanide complexes with CF_3SO_3Me and subsequent recrystallization led to the respective μ-aminocarbyne derivatives $[Ru_2Cp_2(CO)_2(L)\{\mu\text{-}CNMe(CH_2Ph)\}]CF_3SO_3$ (L = CO, $[\mathbf{2h}]^+$, or CNBn), in moderate yields.[44,45,46] So far, the latter constitute the only examples for which spectroscopic (IR, ^{1}H NMR) and X-ray crystallographic data have been provided. Related complexes bearing dimethyl- and (methyl)xylyl- substituted μ-aminocarbyne have been reported ($[\mathbf{2a}]^+$ and $[\mathbf{2c}]^+$, respectively), but details about their preparation and characterization were not given.[47]

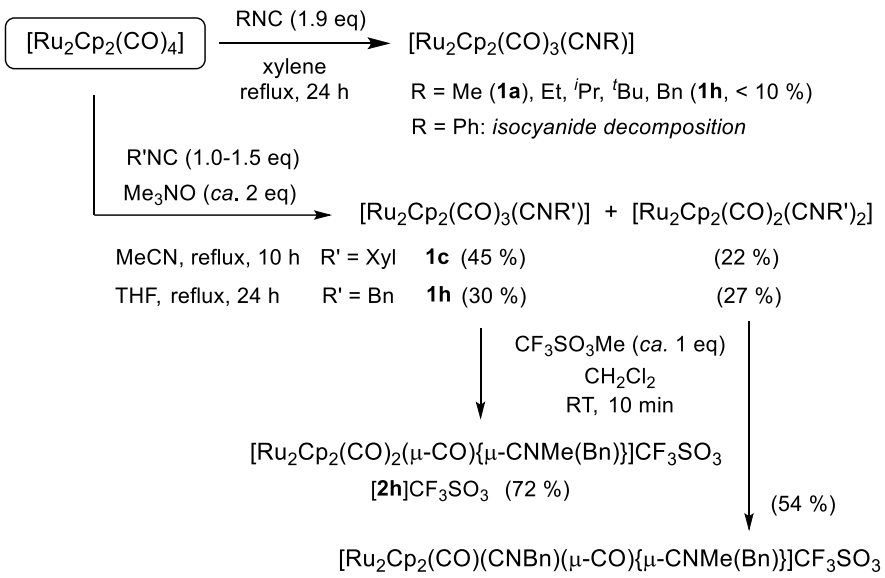

Scheme 2. Overview of previously reported reactivity of $[Ru_2Cp_2(CO)_4]$ to obtain mono-isocyanide and aminocarbyne complexes. Isolated yields in parenthesis, when available. Isocyanide naming (**a-h**) is given in Scheme 1.

2. Results and discussion

2.1. Synthesis and characterization of diruthenium aminocarbyne complexes

In the attempt to expand the recently-developed synthesis of diiron aminocarbyne complexes (Scheme 1) to diruthenium homologues, the reactivity of $[Ru_2Cp_2(CO)_4]$ with a series of alkyl and aryl isocyanides was initially assessed in MeCN by IR spectroscopy (Scheme 3a). Reactions with equimolar amounts of methyl, cyclohexyl (Cy), xylyl (Xyl) or 1*H*-indol-5-yl (Ind) isocyanide at room temperature led to the slow formation of the expected mono-substituted products $[Ru_2Cp_2(CO)_3(CNR)]$ (R = Me, **1a**; R = Cy, **1b**; R = Xyl, **1c**; R = Ind, **1d**). The yields are significantly affected by the nature of the isocyanide substituent (R), decreasing along the series Cy > Me > Xyl > Ind, as indicated by the relative intensities of the carbonyl bands due to **1a-d** and $[Ru_2Cp_2(CO)_4]$ in the final reaction mixture (Figure S1). Conversely, $[Ru_2Cp_2(CO)_4]$ was unreactive towards other seven alkyl and aryl isocyanides (including benzyl isocyanide) in MeCN, both at room temperature and at reflux (see notes [48,49]). Besides, spectral

changes in the 2000-2700 cm^{-1} region were recognized, possibly related to some reactions involving the isocyanides. Overall, these results are in accordance with the literature in that $[Ru_2Cp_2(CO)_4]$ is sluggish to undergo thermal carbonyl/isocyanide substitution. Concurrent isocyanide decomposition may represent another limiting factor.[43] Therefore, alternative conditions employing Me_3NO as CO scavenger were explored, starting from the published preparations of **1c**[46] and **1h**[44] (Scheme 2). Thus, $[Ru_2Cp_2(CO)_3\{CN(2\text{-naphthyl})\}]$, **1e**, was prepared in a modest yield using a large excess (4 eq.) of Me_3NO in refluxing THF (Scheme 3b). Comparatively lower amounts of $[Ru_2Cp_2(CO)_3(CNR)]$ (R = 4-C_6H_4OMe, **1f**; R = CH(Me)Ph, **1g**) were afforded from 4-methoxyphenyl isocyanide and (S)-α-methylbenzyl isocyanide (Figure S2). In general, increasing the temperature and the Me_3NO/Ru molar ratio led to a higher conversion of $[Ru_2Cp_2(CO)_4]$, at the expense of selectivity. Note that a significant fraction of disubstituted products, $[Ru_2Cp_2(CO)_2(CNR)_2]$ (R = Bn, Xyl), was previously isolated under the same experimental conditions, Scheme 2.[46,44]

The crude mixtures containing **1a-b** and **1d-h** were treated with methyl triflate in CH_2Cl_2 solution, to access the cationic μ-aminocarbyne complexes $[Ru_2Cp_2(CO)_2(\mu\text{-}CO)\{\mu\text{-}CNMe(R)\}]^+$, [**2a-h**]$^+$ (Scheme 3c). Differently, **1c** was purified taking advantage of its poor solubility in MeCN (see Experimental) and then it was methylated in CH_2Cl_2. We noticed that using an excess of methyl triflate (≥ 1 eq. with respect to the $[Ru_2Cp_2(CO)_4]$ starting material) led to a drop in the yield of [**2**]$^+$. Therefore, the methylating agent was added proportionally to the yield of the CO/isocyanide exchange in the first step (0.50-0.95 eq.). Products [**2a-g**]CF_3SO_3 were purified by careful alumina chromatography, operating in air using common (wet) solvents. Unreacted $[Ru_2Cp_2(CO)_4]$ was eluted with CH_2Cl_2 and recovered (see ESI). Elution with THF or CH_2Cl_2/THF mixtures allowed the collection of an orange band, containing mainly $[RuCpCl(CO)_2]$, according to the characteristic infrared carbonyl bands.[50] This half-sandwich ruthenium(II) compound is likely formed via oxidative cleavage of $[Ru_2Cp_2(CO)_3(CE)]$ (E = O, NR).[50,51] Yellow bands containing [**2b-g**]CF_3SO_3 were collected with MeCN while a MeOH/THF mixture was used to separate [**2a**]CF_3SO_3. In fact, alumina-catalysed carbonyl/acetonitrile exchange occurred during

the elution of [**2a**]$^+$ with MeCN, affording [$Ru_2Cp_2(CO)(CNMe)(\mu\text{-}CO)(\mu\text{-}CNMe_2)$]$^+$, [**3a**]$^+$, as checked by its independent preparation from [**2a**]$^+$ and $Me_3NO{\cdot}2H_2O$ in MeCN (Scheme 4). Notably, the diiron analogue [**2a**^{Fe}]$^+$ withstand alumina chromatography with MeCN[29] and no MeCN/CO exchange was observed in a MeCN solution of [**2a**]CF_3SO_3 at room temperature.

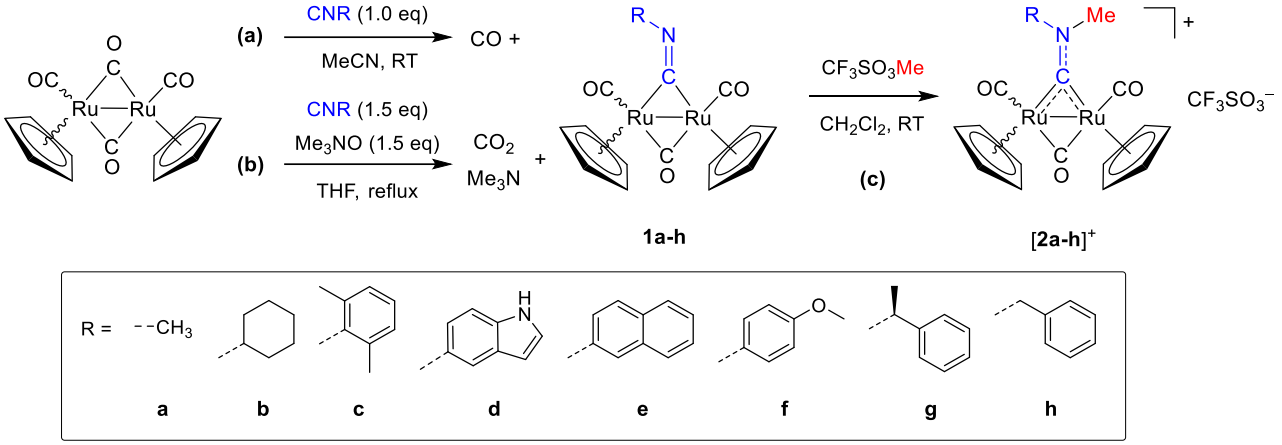

Scheme 3. Synthesis of diruthenium isocyanide complexes **1a-h** from [$Ru_2Cp_2(CO)_4$] by direct (**a**) or Me_3NO-assisted (**b**) CO/CNR replacement (only one form of the fluxional complexes [$Ru_2Cp_2(CO)_3(CE)$], E = O, NR, is depicted for simplicity). Synthesis of diruthenium μ-aminocarbyne complexes [**2a-h**]$^+$ as triflate salts by methylation of the isocyanide ligand in **1a-h**. Wavy bonds represent *cis*/*trans* isomerism. RT = room temperature.

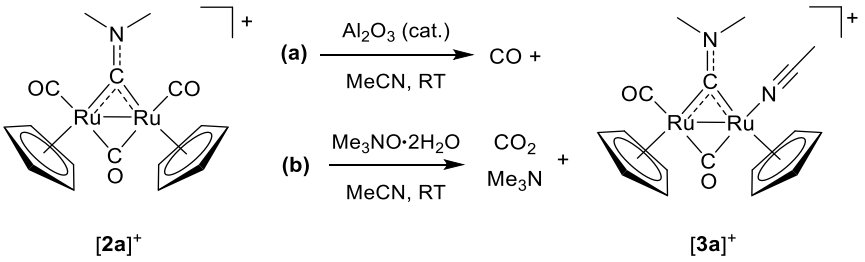

Scheme 4. Formation of [$Ru_2Cp_2(CO)(NCMe)(\mu\text{-}CO)\{\mu\text{-}CNMe_2\}$]$^+$, [**3a**]$^+$, by CO/MeCN replacement promoted by neutral alumina (**a**) or by Me_3NO (**b**). Complexes isolated as $CF_3SO_3^-$ salts. RT = room temperature.

Compounds [**2a-g**]CF_3SO_3 were isolated as air-stable yellow (**a-d**) or yellow-brown (**e-g**) solids, the latter containing some impurities. The overall yield, with respect to [$Ru_2Cp_2(CO)_4$], is heavily influenced by the CO/CNR replacement in the first stage, decreasing in the series: [**2b**]$^+$ (86 %) > [**2a**]$^+$ (66 %) > [**2c**]$^+$ (50 %) > [**2d-e**]$^+$ (≈ 23 %) > [**2f**]$^+$ ≈ [**2g**]$^+$. Multiple preparations of [**2b**]CF_3SO_3 on a 1-gram scale gave a consistent 86 % yield of the pure product.

Compounds [**2a-g**]CF_3SO_3 were characterized by elemental (CHNS) analyses, IR (solid state, CH_2Cl_2 and MeCN solutions) and NMR (acetone-d_6 or $CDCl_3$ solutions) spectroscopy.[52] IR and NMR spectra are displayed in Figures S3-S26 and selected IR and NMR data are compared with those of the diiron homologues [$\mathbf{2}^{\mathbf{Fe}}$]$^+$ in Tables S1-S2. As assessed by ^{1}H NMR spectroscopy, the diruthenium μ-aminocarbyne complexes [**2a-e**]$^+$ were obtained as mixtures of *cis*- and *trans*- isomers. This kind of isomerism arises from the relative orientation of the cyclopentadienyl ligands around the $M_2(\mu\text{-}C)_2$ unit (M = Fe, Ru) and is relatively rare for iron complexes.[53] The *cis* stereochemistry of the major isomer of [**2b-d**]$^+$ was assessed by ^{1}H NOESY measurements. *Trans* isomers eluted first during alumina chromatography and possess a higher solubility in diethyl ether (and in water - *vide infra*) used in the last stage of the workup, resulting in a rather low amount (2-7 %) in the final products. *Trans* to *cis* isomerization in [**2a,b,e**]$^+$ was achieved in refluxing isopropanol.

The IR spectra in CH_2Cl_2 or MeCN solutions of [**2a-g**]$^+$ show IR bands around 2025 (s), 1992 (w) and 1842 (s) cm^{-1} due to the carbonyl ligands and a medium-intensity absorption in the 1540-1614 cm^{-1} range related to the C(carbyne)-N stretching. The three carbonyl bands appear of similar intensity and shifted to lower wavenumbers in the solid state. The change from iron to ruthenium in $[M_2Cp_2(CO)_2(\mu\text{-}CO)\{\mu\text{-}CNMe(R)\}]^+$ complexes (M = Fe, [$\mathbf{2a\text{-}h}^{\mathbf{Fe}}$]$^+$; Ru, [**2a-h**]$^+$) determines a shift of carbonyl and C(carbyne)-N stretching vibrations to higher wavenumbers (+ 2-6 and 6-12 cm^{-1}, respectively)~~, reflecting a slight decrease in backdonation from the metal centre~~.[46] This is coherent with the general observation of a higher degree of π-backdonation from 3d metals in low oxidation states to π-acceptor ligands, compared to the homologous 4d metal based systems.[54,55,56]

The $^{13}C\{^1H\}$ NMR spectra of [**2a-d**]$^+$ show resonances around 295-300, 228-231 and 196-198 ppm for the bridging carbyne, the bridging carbonyl and the terminal carbonyls, respectively. These unprecedented $^{13}C\{^1H\}$ NMR data allow to observe a peculiar upfield shift of the resonances of the $[M_2(CO)_2(\mu\text{-}CO)\{\mu\text{-}CN\}]$ core on going from Fe to Ru (μ-CO and μ-CN: − 22/26 ppm, t-CO: − 12 ppm).[31,57] The structures of [**2a-d**]CF_3SO_3 and [**2g**]CF_3SO_3 were ascertained by X-ray diffraction on

single crystals (Figure 1 and Table 1). All these cationic complexes display a *cis*-[$Ru_2Cp_2(CO)_2(\mu\text{-}CO)$] core bonded to a bridging μ-CN(Me)(R) aminocarbyne ligand. The structures of [**2a-d,g**]$^+$ are very similar to that of [**2h**]$^+$, which was the only [$Ru_2Cp_2(CO)_2(\mu\text{-}CO)\{\mu\text{-}CN(Me)(R)\}$]$^+$ complex structurally characterized prior to this work.[46] Both bridging ligands, that is, μ-CO and μ-CN(Me)(R), are symmetrically bonded to the two Ru centres, and the C(4)-N(1) distances (Table 1) fall in the typical range for an iminium bond.[58]

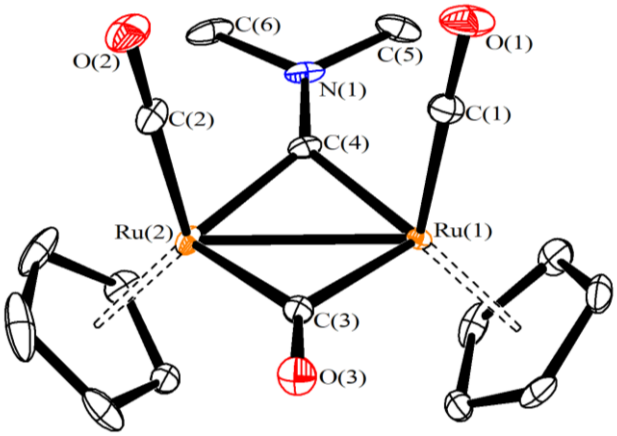

[**2a**]$^+$

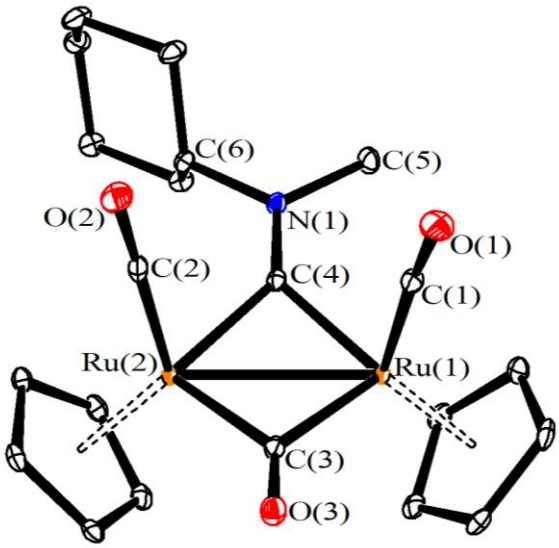

[**2b**]$^+$

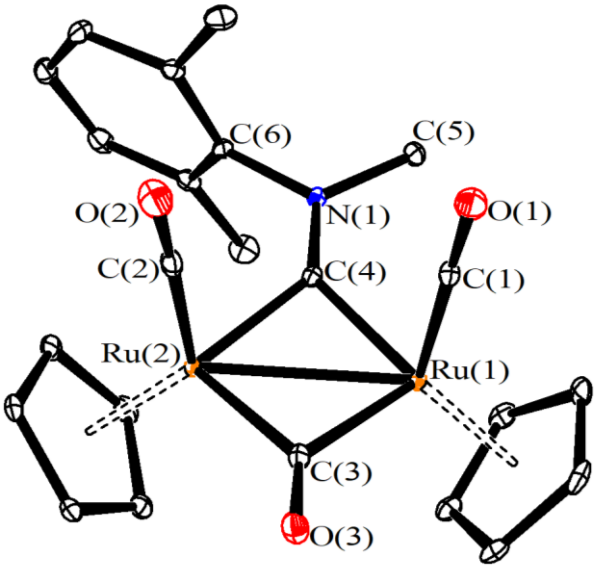

[**2c**]$^+$

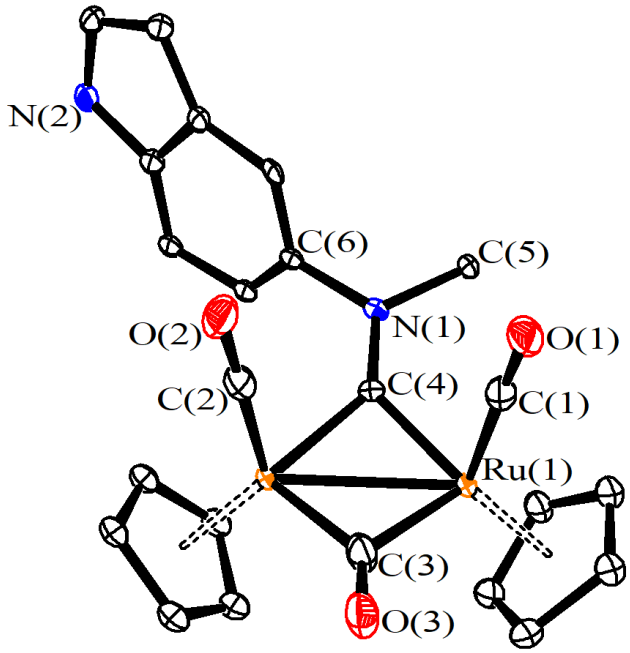

[**2d**]$^+$

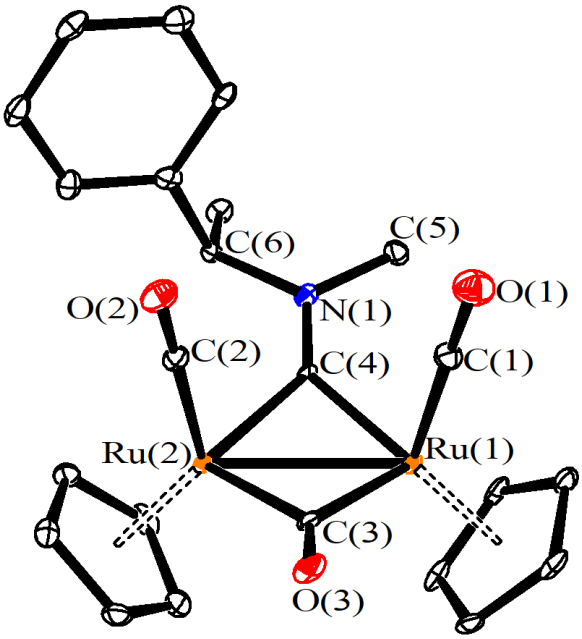

[**2g**]$^+$

Figure 1. Molecular structures of [**2a-d**]$^+$ and [**2g**]$^+$ (triflate salts). Displacement ellipsoids are at the 30% probability level. Hydrogen atoms have been omitted for clarity.

Table 1. Selected bond lengths (Å) and angles (°) for [**2a-d**]$^+$ and [**2g**]$^+$.

	[**2a**]$^+$	[**2b**]$^+$	[**2c**]$^+$	[**2d**]$^+$	[**2g**]$^+$
Ru(1)-Ru(2)	2.7186(3)	2.7197(2)	2.72416(19)	2.681(3)	2.7129(15)
Ru(1)-C(1)	1.873(3)	1.8825(19)	1.8896(16)	1.87(3)	1.891(7)
Ru(2)-C(2)	1.878(3)	1.8814(19)	1.8855(17)	1.86(3)	1.888(7)
Ru(1)-C(3)	2.066(2)	2.0469(18)	2.0554(15)	2.07(3)	2.030(7)
Ru(2)-C(3)	2.043(2)	2.0585(17)	2.0572(15)	2.05(3)	2.054(8)
Ru(1)-C(4)	1.995(2)	1.9984(17)	1.9894(15)	1.96(2)	1.993(7)
Ru(2)-C(4)	1.992(3)	1.9973(17)	1.9943(15)	1.98(2)	1.996(7)
C(1)-O(1)	1.142(3)	1.141(2)	1.137(2)	1.09(3)	1.132(10)
C(2)-O(2)	1.138(3)	1.139(2)	1.137(2)	1.14(3)	1.128(9)
C(3)-O(3)	1.163(3)	1.167(2)	1.163(2)	1.14(3)	1.191(10)
C(4)-N(1)	1.285(3)	1.286(2)	1.2956(19)	1.28(3)	1.304(10)
Ru(1)-C(1)-O(1)	178.4(3)	174.61(16)	179.47(15)	178(3)	178.5(8)
Ru(2)-C(2)-O(2)	179.6(3)	178.69(16)	176.91(15)	175(3)	175.8(7)
Ru(1)-C(3)-Ru(2)	82.85(9)	82.98(7)	82.97(6)	81.2(10)	83.3(3)
Ru(1)-C(4)-Ru(2)	85.95(9)	85.79(7)	86.29(6)	85.6(10)	85.7(3)
C(4)-N(1)-C(5)	123.0(2)	121.42(15)	123.46(13)	122(2)	121.1(6)
C(4)-N(1)-C(6)	122.2(3)	121.64(15)	120.57(13)	123(2)	119.7(6)
C(5)-N(1)-C(6)	114.8(2)	116.85(14)	115.95(12)	115(2)	119.2(6)

2.2. Solubility and stability in aqueous solutions, and octanol-water partition coefficients

The solubility and octanol-water partition coefficient (Log P_{ow}) of [**2a-e,h**]CF_3SO_3 were assessed by ^{1}H NMR and UV-vis methods (see Table 2, and Experimental for details). All the salts are soluble in water in the low millimolar range ($0.1\text{-}2.0\cdot10^{-3}$ mol/L). Saturated solutions of [**2a-d**]CF_3SO_3 in D_2O are enriched in the *trans*-isomers with respect to what is observed in acetone-d_6 and $CDCl_3$, where the compounds are highly soluble, suggesting that the *trans*-isomers are more soluble in water.[59] Notably, 20 % of *trans*-[**2a**]$^+$ and 30 % of *trans*-[**2b**]$^+$ were detected in D_2O (Figures S27-S29). The dimethyl-substituted aminocarbyne [**2a**]CF_3SO_3 features the highest water solubility and the lowest Log P_{ow}, while the presence of 2-naphthyl as *N*-substituent results in the least soluble and most lipophilic compound of the series. Nevertheless, all the compounds can be considered as *amphiphilic* ($-1 \leq \text{Log } P_{ow} \leq 1$). As a general remark, [**2a-e,h**]CF_3SO_3 are less water soluble and slightly more lipophilic if compared to their

diiron counterparts (Table S3). A striking difference in solubility trends between Fe and Ru analogues on varying the nitrogen substituent is represented by the cyclohexyl derivatives (order of decreasing solubility, Fe: ***Cy*** > Me ≈ Bn > Xyl > Ind > Naph; Ru: Me > Xyl ≈ Bn > ***Cy*** > Ind > Naph).

Next, D_2O/CD_3OD solutions of [**2a-e,h**]CF_3SO_3 were maintained at 37 °C for 72 h and analysed by ^1H NMR. Parallel experiments were conducted on [**2a-d**]CF_3SO_3 using a deuterated cell culture medium (DMEM-d), to simulate the conditions employed for the biological tests (*vide infra*). Remarkably, the compounds were totally inert in all the tested conditions (≥ 99 % starting material detected at the end of the experiment, Figure S30). No change was detected even when an aqueous (D_2O) solution of [**2b**]CF_3SO_3 was heated at reflux temperature for 12 h. This behaviour is relatively uncommon in organometallic chemistry, and in particular when considering the metal-cyclopentadienyl[60,61] and metal-CO linkages,[62] that may slowly decay in aqueous solutions. As a pertinent comparison, consider that the diiron complexes $[\mathbf{2}^{\mathbf{Fe}}]^+$ undergo a slow, progressive fragmentation at 37 °C in aqueous media, resulting in the elimination of CO and cyclopentadiene, along with the precipitation of iron(III) oxides.[30,63]

The superior stability of the diruthenium framework $[\mathbf{2}]^+$ appears to result from a combination of the enhanced stability of the Ru_2Cp_2 core in comparison to Fe_2Cp_2[64,65] and the conjugation of the cyclopentadienyl ligands, acting as π-donors, with three CO ligands and tightly bound aminocarbyne moiety, possessing significant π-acceptor properties.[28]

In conclusion, all the considered diruthenium μ-aminocarbyne complexes exhibit ideal characteristics for biological applications, including an outstanding stability. However, only those compounds that were obtained in high purity, *i.e.* [**2a-d**]CF_3SO_3, were selected for the cell studies (section 3).

Table 2. Solubility and *cis*/*trans* ratio in water (D_2O), and octanol/water partition coefficients (Log P_{ow}) of diruthenium μ-aminocarbyne compounds.

Compound	**Solubility / M (D_2O) [a]**	***cis*/*trans* ratio (D_2O)**	**Log P_{ow} [a]**
[**2a**]CF_3SO_3	$2.3 \cdot 10^{-3}$	4.5	– 1.07 ± 0.08

[**2b**]CF_3SO_3	$7.8 \cdot 10^{-4}$	2.5	0.06 ± 0.01
[**2c**]CF_3SO_3	$1.6 \cdot 10^{-3}$	25	0.05 ± 0.03
[**2d**]CF_3SO_3	≈ $2 \cdot 10^{-4}$ [b]	11	0.10 ± 0.02
[**2e**]CF_3SO_3	≈ $1 \cdot 10^{-4}$ [b]		0.74 ± 0.03
[**2h**]CF_3SO_3	$1.1 \cdot 10^{-3}$		0.11 ± 0.03

[a] Referred collectively to the *cis* / *trans* mixture of isomers. [b] Below the lowest quantitation value ($3 \cdot 10^{-4}$ mol/L).

2.3. Electrochemistry

We provide a rare electrochemical description of diruthenium bis-cyclopentadienyl compounds.[41,42,66] The redox properties of [**2b**]$^+$ and [**2c**]$^+$, as representative examples, were elucidated by cyclic voltammetry in CH_2Cl_2 and in aqueous phosphate buffer solution. Peak potentials for the observed electron transfers are compiled in Table 3, while CV profiles in CH_2Cl_2/[N^nBu_4]PF_6 are shown in Figures S31-S32. In the positive potential range, the two complexes show one irreversible oxidation that involves two electrons at almost identical potentials (+1.60 and +1.65 V for [**2b**]$^+$ and [**2c**]$^+$, respectively). In the negative potential range, one partially reversible monoelectronic reduction at the formal potential of –1.35 V (i_b/i_f = 0.5 at 0.2 V s^{-1}) is followed by a second irreversible reduction at –1.68 V for [**2b**]$^+$. Instead, only one reduction (E = – 1.37 V), complicated by very fast subsequent reactions (i_b/i_f = 0.54 at 2.0 V s^{-1}), is observed for [**2c**]$^+$.

On the other hand, in the aqueous solvent, the oxidation process of [**2b**]$^+$ and [**2c**]$^+$ is irreversible, multielectronic and shifted to lower potentials (about 300-400 mV) with respect to the organic solvent, whereas an irreversible reduction is observed at potential values comparable to those measured in CH_2Cl_2. Previous CV studies on diiron μ-aminocarbyne complexes [$\mathbf{2a^{Fe}}$]CF_3SO_3 and [$\mathbf{2c^{Fe}}$]CF_3SO_3 were carried out in MeCN [67] and we recently investigated the redox behaviour of several diiron μ-aminocarbyne complexes bearing different *N*-substituents both in CH_2Cl_2 and phosphate buffer;[68] data for [$\mathbf{2b^{Fe}}$]CF_3SO_3 are included in Table 3 for comparison. One oxidation process, which involves two electrons and is partially chemically reversible, is observed at +1.40 V, and is probably associated to the

oxidative cleavage of the iron(I)-iron(I) bond.[69] In the negative potential range, a chemically reversible monoelectronic reduction was observed at the formal potential of – 0.96 V. Hence, the replacement of the Fe^{I} centres by Ru^{I}, with the same *N*-substituent (cyclohexyl), makes the compound more stable towards both the reduction (about 400 mV) and the oxidation (about 200 mV). Anyway, the reduction and oxidation potentials of [**2b**]$^{+}$ and [**2c**]$^{+}$ are out of the biologically relevant range of potentials, that approximately cover the window –0.4 to +0.8 V *vs*. SHE (–0.6 to +0.6 V *vs*. Ag/AgCl).[70] Remarkably, the electrochemical properties of [**2b**]$^{+}$ and [**2c**]$^{+}$ are similar, indicating a minor influence of the aminocarbyne substituent (Cy or Xyl). Analogous conclusions may be traced for other members of this family of compounds, e.g. [**2a**]$^{+}$ and [**2d**]$^{+}$.

Table 3. Formal electrode potentials (V, *vs* Ag/AgCl and, in brackets, *vs* $FeCp_2$) and peak-to-peak separations (mV) for the redox changes exhibited in CH_2Cl_2/[N^nBu_4]PF_6 0.2 M and in aqueous media by [**2b,c**]CF_3SO_3 and by the diiron analogue [**2b^{Fe}**]CF_3SO_3 for comparison.

Compound	Electrolyte [a]	Oxidation process		Reduction process		
		$E°'_1$	ΔE[b]	$E°'_2$	ΔE[b]	$E°'_3$
[**2b**]CF_3SO_3	CH_2Cl_2/[Bu_4N]PF_6	+1.60[c] (+1.15)		–1.35 (–1.80)	105	–1.68[c] (–2.13)
	PB/H_2O	+1.31[c] (+1.11)		–1.38[c] (–1.58)		
[**2c**]CF_3SO_3	CH_2Cl_2/[Bu_4N]PF_6	+1.65[c] (+1.20)		–1.37[c] (–1.82)		
	PB/H_2O	+1.25[c] (+1.05)		–1.33[c] (–1.53)		
[**2b^{Fe}**]CF_3SO_3	CH_2Cl_2/[Bu_4N]PF_6	+1.40 (+0.95)	120	–0.96 (–1.41)	84	
	PB/H_2O	+1.10[c] (+0.90)		–0.99 (–1.19)	100	

[a] PB = phosphate buffer (pH = 7.3). [b] Measured at 0.1 V·s^{-1}. [c] Peak potential value for irreversible processes.

2.4. Biological studies

2.4.1. Cytotoxicity

The initial screening for in vitro cytotoxicity of [**2a-d**]CF_3SO_3 was conducted on A2780, A2780R, and MCF-7 human cancer cell lines (Table 4). Cisplatin and RAPTA-C[71] served as positive and negative controls, respectively. Complex [**2a**]$^{+}$ was inactive up to the tested 50 μM concentration, similar to

previous findings for the related diiron complex [**2a**$^{\mathbf{Fe}}$]$^+$.[31] This inactivity serves as indirect evidence for the non-toxicity of the triflate anion, as has been previously observed for various organometallic salts.[72,73] In contrast to [**2a**]$^+$, [**2b-d**]$^+$ exhibited substantial cytotoxicity, with [**2d**]$^+$ emerging as the most potent species in this series. Specifically, [**2d**]$^+$, containing an indolyl substituent on the aminocarbyne moiety, showed considerably higher activity than cisplatin across all investigated cancer cell lines. Both [**2b**]$^+$ and [**2d**]$^+$ proved to be much more effective than cisplatin against the cisplatin-resistant A2780R (ovarian cancer) cell line. Based on these preliminary results, [**2d**]CF_3SO_3 was selected for further experiments on additional human cancer cell lines (i.e., HOS, A549, PANC1, CaCo2, PC3 and HeLa). Notably, [**2d**]$^+$ was found to be more effective than cisplatin against all the mentioned cancer cells (Table 4). Furthermore, the cytotoxicity of all diruthenium complexes was evaluated on normal MRC-5 cells, revealing a notable tendency to selectivity. Remarkably, the sensitivity index (SI), defined as the ratio between the IC_{50} value for the noncancerous MRC-5 cell line and a specific cancer cell line, respectively, reached the impressive values of 10.1 (A2780) and 8.5 (A2780R) in the case of [**2d**]CF_3SO_3. In other words, the superior antiproliferative activity of [**2d**]$^+$ is associated with the highest propension for selectivity among the examined diruthenium compounds. It is important to note that the previously investigated diiron compound [**2d**$^{\mathbf{Fe}}$]CF_3SO_3 possesses closely similar lipophilicity but much more modest in vitro anticancer potential compared to the diruthenium homolog [**2d**]CF_3SO_3.[31] The increased anticancer potential of [**2d**]CF_3SO_3, compared to the analogous compounds [**2b-c**]CF_3SO_3 with almost identical Log P_{ow} values, is unlikely to be attributed to a higher cellular uptake of [**2d**]$^+$. Instead, it is probable that the indolyl fragment within [**2d**]$^+$ plays a significant role in its anticancer activity. This aligns with documented anticancer activity associated with the indole scaffold[74,75,76] and indolyl-decorated transition metal compounds in the literature.[77,78] Comparable antiproliferative effects on MCF-7, A549 and PC3 cell lines (Table 1) were recently identified for Ru(II)-arene iminophosphorane complex ([(η^6-*p*-cymene)Ru($\kappa N,O$-Ph_3P=N-CO-2-N-C_5H_4)]Cl, denoted as Ru-IM)[79] with GI_{50} values in

the range of 2.48 – 3.41 μM after 48 h incubation. Another Ru(II)-arene complex ([(η^6-*p*-cymene)(*N*-(4-chlorophenyl)pyridine-2-carbothioamide)(triphenylphosphine)-ruthenium(II)] chloride triflate was identified as highly effective against human colorectal (HCT116), non-small cell lung (NCI-H460), cervical (SiHa) and colon (SW480) carcinoma cell lines investigated using the sulforhodamine B (SRB) assay with IC50 values in the range of 0.26 – 0.41 μM after 72 h incubation.[80]

Table 4. *In vitro* cytotoxicity of the diruthenium compounds and reference compounds (RAPTA-C, cisplatin) on ovarian (A2780 and cisplatin-resistant A2780R), breast (MCF-7), bone (HOS), lung (A549), pancreatic (PANC1), colorectal (CaCo2), prostate (PC3) and cervical (HeLa) human cancer cell lines, and fetal lung fibroblasts (MRC-5) as normal cell line. Data are expressed as IC_{50} ± SD / μM (MTT method, 24 h incubation time). *n.d.* = not determined.

Compound	A2780	A2780R	MCF-7	HOS	A549	PANC1	CaCo2	PC3	HeLa	MRC-5
[**2a**]CF_3SO_3	> 50	> 50	> 50	*n.d.*	*n.d.*	*n.d.*	*n.d.*	*n.d.*	*n.d.*	> 50
[**2b**]CF_3SO_3	7.4 ± 1.6	7.3 ± 0.1	30.2 ± 4.3	*n.d.*	*n.d.*	*n.d.*	*n.d.*	*n.d.*	*n.d.*	48.2 ± 1.3
[**2c**]CF_3SO_3	8.9 ± 0.7	19.3 ± 0.5	45.5 ± 3.8	*n.d.*	*n.d.*	*n.d.*	*n.d.*	*n.d.*	*n.d.*	> 50
[**2d**]CF_3SO_3	3.7 ± 0.1	4.4 ± 1.0	13.0 ± 1.7	12.7 ± 2.6	16.3 ± 3.0	9.7 ± 2.5	20.3 ± 2.4	10.4 ± 2.6	10.4 ± 1.5	37.4 ± 3.8
RAPTA-C	> 50	*n.d.*	*n.d.*	> 50	> 50	> 50	> 50	> 50	> 50	*n.d.*
Ru-IM*	*n.d.*	*n.d.*	2.48	*n.d.*	3.41	*n.d.*	*n.d.*	2.66	*n.d.*	*n.d.*
cisplatin	15.2 ± 1.1	40.0 ± 3.9	28.4 ± 2.7	26.3 ± 3.3	39.2 ± 3.1	> 50	> 50	> 50	30.7 ± 0.6	> 50

*The GI_{50} data (μM) for the compound Ru-IM in sulforhodamine B assay after 48 h incubation were adopted from Ref. 79.

The most cytotoxic compound [**2d**]CF_3SO_3, along with RAPTA-C and cisplatin for comparative purposes, was chosen to investigate the time-dependency (24, 48 and 72h incubation time) of *in vitro* cytotoxicity against A2780 cells. Results are summarized in Table 5, revealing that IC_{50} of [**2d**]CF_3SO_3 remains substantially unvaried within the specified time window, whilst the IC_{50} related to cisplatin slightly decreases over time. This outcome outlines that [**2d**]CF_3SO_3 exerts its activity mainly within the initial 24 h of incubation, indicating significant differences in the targets and mechanisms of action between [**2d**]CF_3SO_3 and cisplatin, respectively.

Table 5. Time dependence of *in vitro* cytotoxicity of [**2d**]CF_3SO_3 and reference compounds (RAPTA-C, cisplatin) against A2780 cells (24h, 48h and 72h incubation time). Data are expressed as IC_{50} ± SD / μM (MTT method).

Compound	24 h	48 h	72 h
[**2d**]CF_3SO_3	4.9 ± 1.1	3.5 ± 0.5	3.0 ± 0.2
RAPTA-C	> 50	> 50	> 50
cisplatin	15.2 ± 1.1	12.4 ± 1.8	5.8 ± 1.8

2.4.2. Cellular ruthenium uptake

The cellular uptake of ruthenium was evaluated in A2780 cells exposed to [**2a**]CF_3SO_3 and [**2d**]CF_3SO_3 at their respective IC_{50} concentrations, during 72 h incubation (at 2, 6, 12, 24, 48, and 72 h time points) (Figure 2). The results reveal similar dynamics of internalization for both complexes, showing a steep increase in intracellular Ru content within the initial 24h, particularly for [**2d**]CF_3SO_3, which is applied at a 13.5-fold lower concentration. Subsequently, the ruthenium level remains relatively constant during the successive 24h, before experiencing further increase up to 72h. In contrast, the uptake of ruthenium from the reference compound RAPTA-C is rather slow and limited, consistent with existing literature.[81] It is noteworthy that [**2a**]CF_3SO_3 and [**2d**]CF_3SO_3 exhibit different lipophilicity (Table 2), which correlated with strikingly different antiproliferative activities (Table 4). Based on the Ru uptake results, it can be inferred that the intracellular localization and pathways of these compounds are likely to differ significantly.

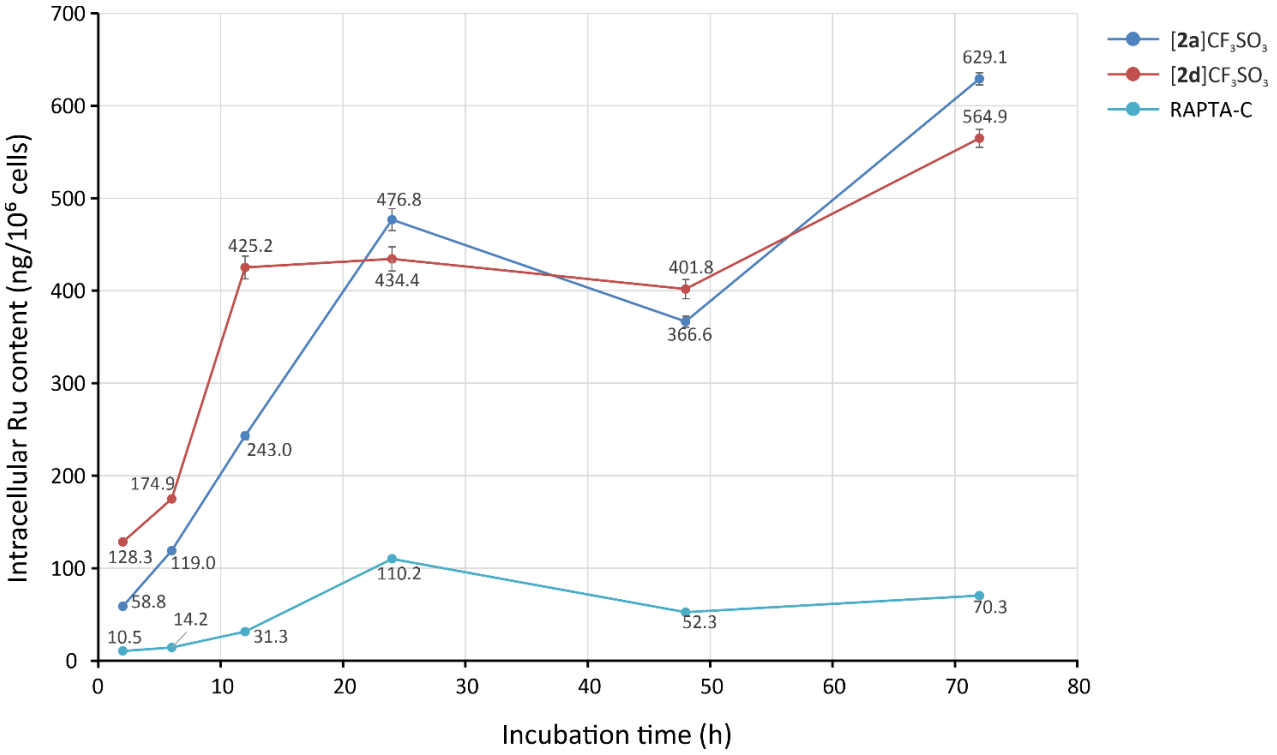

Figure 2. Cellular ruthenium uptake of [**2a**]CF_3SO_3 and [**2d**]CF_3SO_3 and RAPTA-C in A2780 cells as determined by ICP-MS. The complexes were applied at the half-cytotoxic concentrations obtained for A2780 cells after 24h of incubation, *i.e*. at 50 µM concentration for [**2a**]CF_3SO_3 and RAPTA-C, and at 3.7 µM concentration for [**2d**]CF_3SO_3. The indicated values represent the mean intracellular concentration of ruthenium in ng/10^6 cells and were calculated from two parallel determinations.

2.4.3. Interaction with reduced glutathione and bovine serum albumin

Next, we studied the interaction of [**2a**]CF_3SO_3 and [**2d**]CF_3SO_3, with reduced glutathione and bovine serum albumin (BSA) using electrospray-ionization mass spectrometry in positive ionization mode. These experiments complement the cellular uptake data providing information on the affinity of the complexes towards one of the most important cellular antioxidants (reduced glutathione, GSH) and the most abundant protein in mammalian blood plasma. The potential formation of adducts with GSH was evaluated after 2h and 24h of incubation. Mass spectra of mixtures containing [**2a**]CF_3SO_3 and GSH (1:1000 molar ratio) revealed the partial formation of interaction products (Figures S33-S34), while no interaction between [**2d**]CF_3SO_3 and GSH was recognized after 24h incubation (Figure S35). The

observed difference in reactivity between [**2a**]$^{+}$ and [**2d**]$^{+}$ suggests that [**2a**]$^{+}$ could be deactivated by the high intracellular level of GSH.

We moved to examine the potential interaction of the chosen complexes, applied at a final concentration of 1 mM, with BSA (at a final concentration of 30 µM) over a 48h period, using MALDI-MS. The results (Figure S36) clearly show that no appreciable interaction occurred between either of the complexes and bovine serum albumin, even after 48h of incubation.

2.4.4. Cell cycle analysis

The analysis of the cellular cycle in A2780 cells co-incubated with half-cytotoxic concentrations of [**2a**]CF_3SO_3 and [**2d**]CF_3SO_3 for 24h (Figure 3) revealed that only [**2d**]CF_3SO_3, exhibiting a high antiproliferative effect, significantly impacted the cell cycle of A2780 cells. It induced the arrest of the majority of cells in the G0/G1 phase (resting phase) and significantly reduced the cell populations in both the S phase and the G2/M phase of the cell cycle. In contrast, the reference drug cisplatin arrested most cells in the synthetic S phase of the cycle by targeting newly replicated DNA.[82] On the other hand, the non-cytotoxic [**2a**]CF_3SO_3 had virtually no effect on the cellular cycle of A2780 cells.

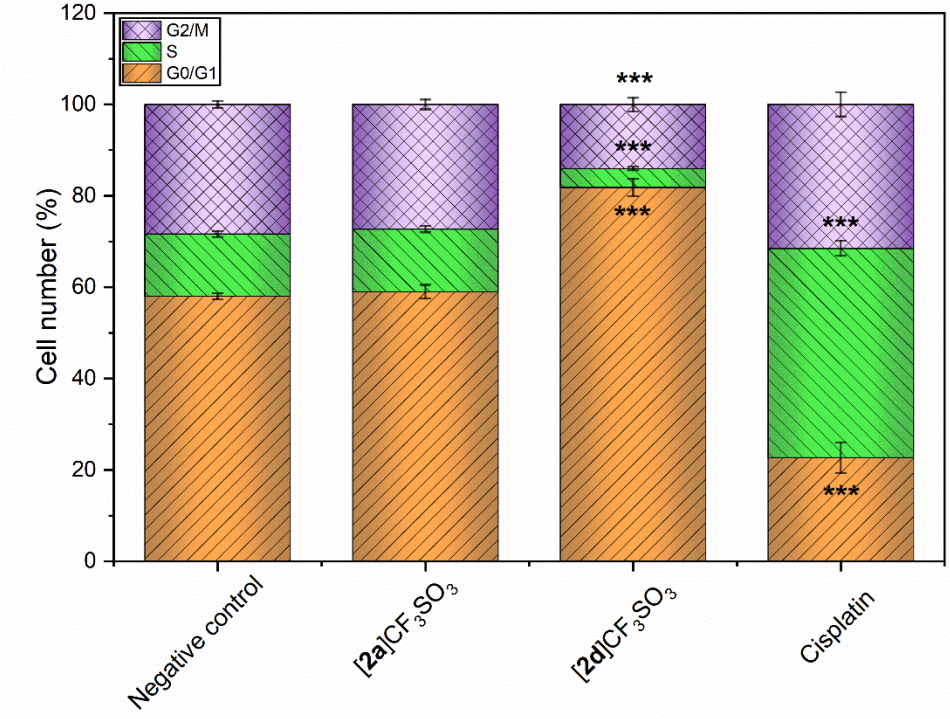

Figure 3. Effects of [**2a**]CF_3SO_3, [**2d**]CF_3SO_3 and cisplatin (applied at the IC_{50} levels 50 μM, and 3.7 μM, respectively) on the cell cycle in A2780 cells after 24h of incubation. Significance levels: * p<0.05, ** p<0.01, *** p<0.005. Negative control represents the untreated cells.

2.4.5. Induction of cell death

The selected complexes [**2a**]CF_3SO_3 and [**2d**]CF_3SO_3 showed no appreciable membrane damage, as indicated by the lack of reactivity towards Annexin V and/or DNA damage revealed by staining with propidium iodide (PI) during the 24h co-incubation with A2780 cells. This observation aligns with the G0/G1 phase arrest demonstrated in the cell cycle modification experiments. In contrast, cisplatin caused significant damage in over 30% of all cells. However, [**2d**]CF_3SO_3 was able to activate executioner caspases 3/7 in the A2780 cells, similar to cisplatin. These results suggest that [**2d**]CF_3SO_3 may act through multiple steps, eliciting different levels of damage to cancer cells. Clearly, the antiproliferative effect of [**2d**]CF_3SO_3, resulting from the suppression of cellular metabolism, is the fastest process. The subsequent phase involves actual damage to cellular structures, as indicated by the activation of Cas 3/7.

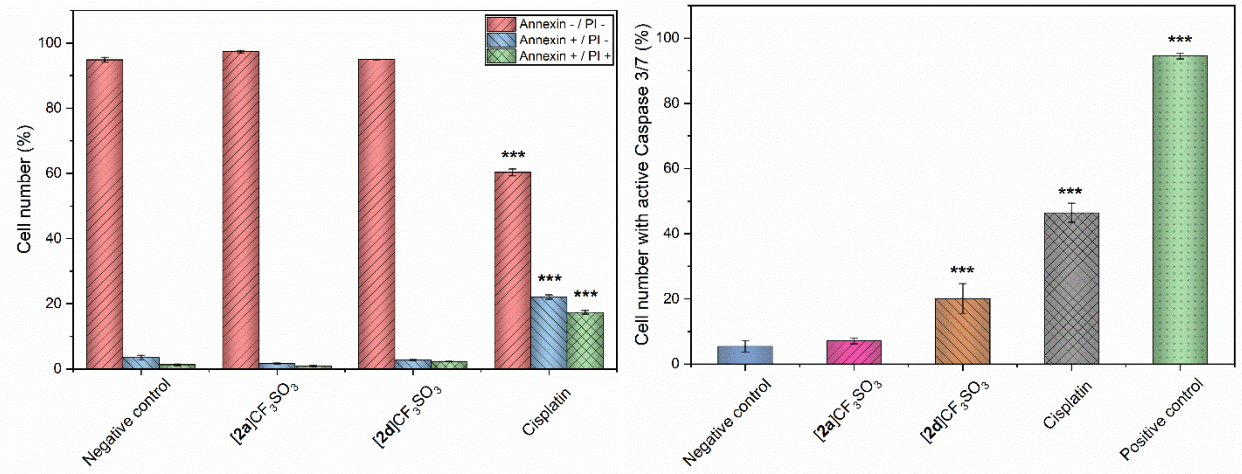

Figure 4. Effects of [**2a**]CF_3SO_3, [**2d**]CF_3SO_3 and cisplatin (24 h incubation, applied at the IC_{50} levels 50 μM, and 3.7 μM, respectively) on the cell death induction in A2780 cells (left) and effector caspases 3/7 activation in A2780 cells (right). Positive control represents heat damaged cells (60 °C/10min.) and the negative control represents untreated cells. Significance levels: * p<0.05, ** p<0.01, *** p<0.005.

2.4.6. Induction of autophagy

Autophagy is usually associated with natural recycling processes in normal cells, as well as with metabolic and environmental stress leading to cell death in the initial stages of tumorigenesis. However, in advanced stages of tumorigenesis, autophagy may function as tumour-promoting mechanism by sustaining cancer cell survival in stressful microenvironments.[83] Several mechanisms are linked to autophagy induction by cytotoxic agents, including the induction/promotion of intracellular oxidative stress and moderation of mTOR activity.[84] Our results highlight a significant effect of [**2d**]CF_3SO_3 and cisplatin on the activation of autophagy in A2780 cells (Figure 5). These findings align with our working hypothesis that the mechanism of action of [**2d**]CF_3SO_3 is diphasic. This compound induced metabolic stress and halted the proliferation in the first (fast) stage, followed by the induction of apoptosis and autophagy in the second (slower) stage.

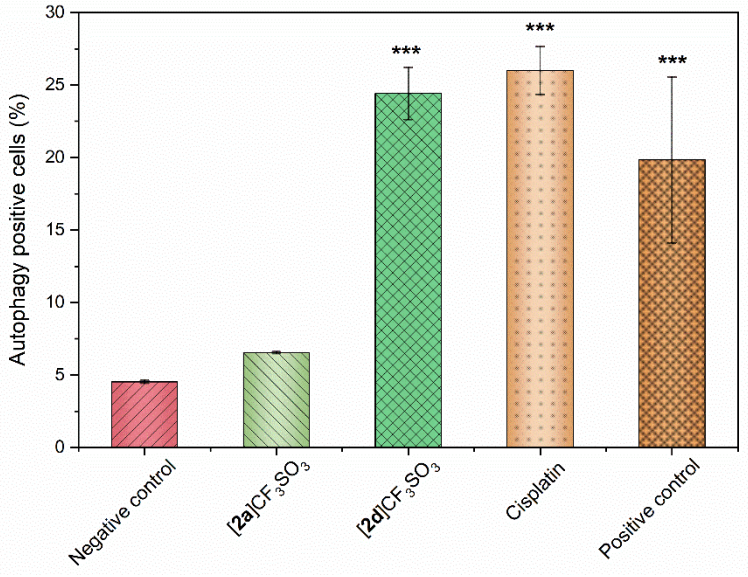

Figure 5. Effects of [**2a**]CF_3SO_3, [**2d**]CF_3SO_3 and cisplatin (24 h incubation, applied at the IC_{50} levels of 50 μM, and 3.7 μM, respectively) on the induction of autophagy in A2780 cells. Positive control: a mixture of chloroquine (10 μM) and rapamycin (0.5 μM). Significance levels: * p<0.05, ** p<0.01, *** p<0.005.

2.4.7. ROS production and mitochondrial membrane potential

Both [**2a**]CF_3SO_3 and [**2d**]CF_3SO_3 slightly increased the levels of reactive oxygen species (ROS) in A2780 cells after 24 hours of incubation. However, no noticeable effect on mitochondrial membrane potential was detected, in contrast to cisplatin, which led to significant depolarization of mitochondrial membranes and their subsequent destruction.[85]

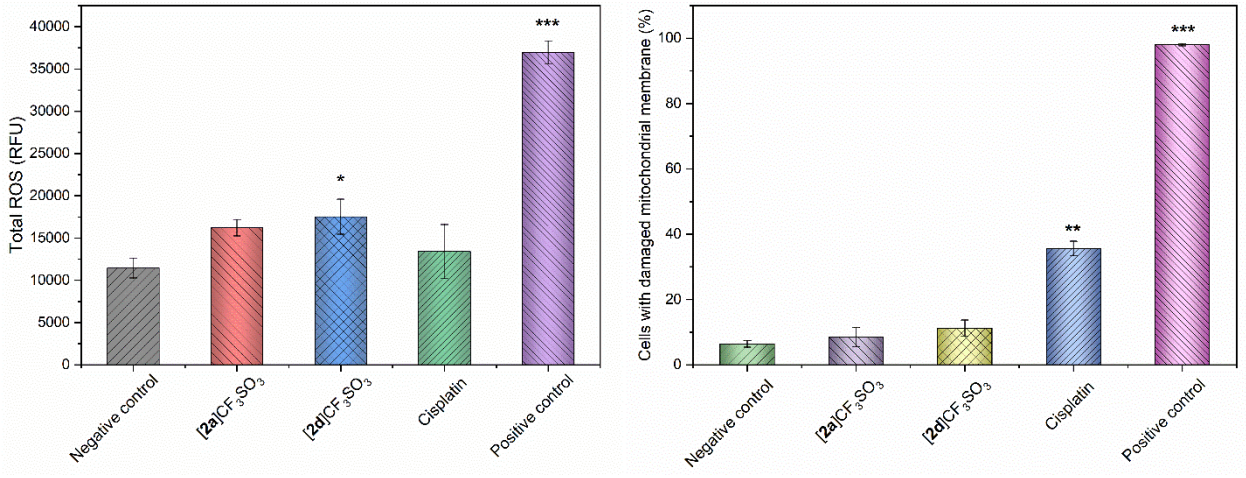

Figure 6. Effects of [**2a**]CF_3SO_3, [**2d**]CF_3SO_3 and cisplatin (24 h incubation, applied at the IC_{50} levels of 50 μM, and 3.7 μM, respectively) on the intracellular ROS levels (*left*, positive control: pyocyanin) and on mitochondrial

membrane potential (right, positive control: CCCP) in A2780 cells. Significance levels: * $p<0.05$, ** $p<0.01$, *** $p<0.005$.

3. Concluding remarks

Carbonyl/isocyanide substitution reactions were systematically investigated on $[Ru_2Cp_2(CO)_4]$, revealing substantial inertness compared to the d-block first-row analogue $[Fe_2Cp_2(CO)_4]$. However, we present straightforward procedures for the preparation of four cationic aminocarbyne derivatives with a rare combination of desired pre-requisites for drug development, including: 1) presence of a relatively nontoxic metal; 2) appreciable water solubility; 3) balanced hydrophilic/lipophilic character enabling cell uptake; 4) exceptional stability in physiological-like solutions. Cytotoxicity studies, considering a panel of human cancer cell lines, evidenced the crucial effect of the varying aminocarbyne substituent, identifying [**2d**]CF_3SO_3 as the most performant. This complex displays IC_{50} values lower than those obtained with the reference drug cisplatin under the same conditions, along with remarkable selectivity recognized using a noncancerous cell line. The striking behaviour of [**2d**]$^+$ may be ascribable to the favourable biological effects provided by the indolyl moiety, that were previously recognized in other anticancer metal structures. The intracellular Ru uptake data and the observed tendency to full chemical and electrochemical stability, including the absence of easy decomposition pathways upon contact with biomolecules, suggest that the cation [**2d**]$^+$ exerts its activity inside the cells as an intact molecular entity. This activity appears to proceed through a diphasic mechanism, leading to metabolic stress, arresting of cellular proliferation in the first (fast) phase and induction of apoptosis and autophagy in the second (slower) phase. Notably, the physico-chemical properties and the anticancer profile of [**2d**]$^+$ appear markedly different from those of leading organo-ruthenium drug candidates, that are activated through ligand dissociation and primarily exert their activity outside of cells by inhibiting key biomolecules.[17,86,87]

4. Experimental

4.1. General experimental details

$[Ru_2Cp_2(CO)_4]$ was purchased from Merck and stored under N_2. Other reactants and solvents were obtained from Alfa Aesar, Merck, Apollo Scientific or TCI Chemicals and used as received. Methyl isocyanide[88] and $[Ru_2Cp_2(CO)_2(\mu\text{-}CO)\{\mu\text{-}CNMe(Bn)\}]CF_3SO_3$, [**2h**]$CF_3SO_3$,[44] were prepared according to the literature. 1*H*-indol-5-yl isocyanide was prepared from the commercially available 5-amino-indole,[89] the optimized procedure is reported in the ESI. Isocyanides were stored at 4 °C or – 20 °C; contaminated labware was treated with EtOH/HCl. Methyl triflate (≈ 9.1 mol/L) was stored at 4 °C; a diluted solution (≈ 1.8 mol/L) was prepared with anhydrous CH_2Cl_2 and stored under N_2 at 4 °C. All reactions were carried out under N_2 using standard Schlenk techniques. Except for the preparation of [**3a**]CF_3SO_3 (deaerated MeCN), anhydrous solvents stored on 3 Å MS were employed: MeCN was distilled over CaH_2, dry THF and CH_2Cl_2 were obtained from SPS 6 MBRAUN Solvent purifier. All the other operations were conducted under air with common laboratory glassware. Column chromatography was carried out with neutral alumina (Merck). All isolated Ru compounds are air- and moisture- stable in the solid state. NMR spectra were recorded on a Bruker Avance II DRX400 instrument equipped with a BBFO broadband probe. Chemical shifts are referenced to the residual solvent peaks[90] (^1H, ^{13}C) or to external standards[91] (^{19}F to $CFCl_3$). ^1H and $^{13}C\{^1H\}$ spectra were assigned with the assistance of ^1H NOESY (mix time 750 ms, relaxation time 1 sec) and ^1H-^{13}C *gs*-HSQC experiments. $CDCl_3$ stored in the dark over Na_2CO_3 was used for NMR analysis. IR spectra of solid samples (650-4000 cm^{-1}) were recorded on a Perkin Elmer Spectrum One FT-IR spectrometer, equipped with a UATR sampling accessory. IR spectra of solutions were recorded using a CaF_2 liquid transmission cell (1400-2700 cm^{-1}) on a Perkin Elmer Spectrum 100 FT-IR spectrometer. UV-Vis spectra (250-800 nm) were recorded on a Ultraspec 2100 Pro spectrophotometer using PMMA cuvettes (1 cm path length). IR and UV-Vis spectra were processed with Spectragryph.[92] Carbon, hydrogen, nitrogen, and sulfur analyses were performed on a Vario MICRO cube instrument (Elementar).

4.2. Synthesis and characterization of compounds

$[Ru_2Cp_2(CO)_2(\mu\text{-}CO)\{\mu\text{-}CNMe_2\}]CF_3SO_3$, $[\mathbf{2a}]CF_3SO_3$ (Chart 1).

Chart 1. Structure of [**2a**]$^+$.

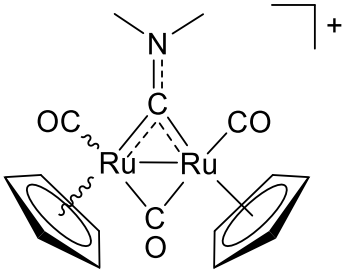

The title compound was previously reported but the synthetic procedure and IR/NMR data were not provided.[93] A yellow solution of $[Ru_2Cp_2(CO)_4]$ (200 mg, 0.45 mmol) in MeCN (8 mL) was treated with freshly-prepared methyl isocyanide (0.08 mL, 0.45 mmol) and stirred at room temperature for 24 h.[94] The formation of $[Ru_2Cp_2(CO)_3(CNMe)]$, **1a**, was checked by IR of the yellow solution (see ESI), and then volatiles were removed under vacuum. The residue was dissolved in CH_2Cl_2 (5 mL) and methyl triflate (1.8 M in CH_2Cl_2; 0.24 mL, 0.43 mmol, 0.95 eq. *vs*. $[Ru_2Cp_2(CO)_4]$)[95] was added dropwise, under vigorous stirring. The yellow solution was stirred at room temperature for 3 h, with progressive formation of a yellow precipitate. The suspension was moved on top of an alumina column (h 4, d 3.4 cm). A yellow band containing unreacted $[Ru_2Cp_2(CO)_4]$ was eluted with CH_2Cl_2 and a yellow-orange band containing $[RuCpCl(CO)_2]$[50] was eluted with THF. Therefore, a bright yellow band containing [**2a**]$^+$ was eluted with THF/MeOH 95:5 *V*/*V* and taken to dryness under vacuum. The residue was triturated in Et_2O and the suspension was filtered. The resulting yellow solid was washed with Et_2O and dried under vacuum (40 °C). Yield: 136 mg, 66 %. Acetonitrile should not be used as eluent for chromatography since it promotes the formation of [**3a**]$^+$ (*see below*) via CO/MeCN exchange. Soluble in EtOH, DMSO, acetone; poorly soluble in CH_2Cl_2, $CHCl_3$, insoluble in Et_2O. X-ray quality crystals of [**2a**]CF_3SO_3 were obtained from slow evaporation of an EtOH solution at room temperature. Anal. calcd. for $C_{17}H_{16}F_3NO_6Ru_2S$: C, 32.85; H, 2.59; N, 2.25; S, 5.16. Found: C, 32.72; H, 2.63; N, 2.23; S, 5.12. IR (solid state): $\tilde{\upsilon}/cm^{-1}$ = 3102w,

2941w, 2011s (CO), 1987s (CO), 1950w-sh, 1834vs (μ-CO), 1794w-sh, 1612m (μ-CN), 1450w, 1430w, 1416w, 1403m, 1274s-sh, 1259s (SO_3), 1226m-sh (SO_3), 1195m, 1154s (SO_3), 1110w, 1062w, 1030s, 1000m-sh, 932w, 846m-sh, 840m, 830m-sh, 767s. IR (CH_2Cl_2): $\tilde{\upsilon}/cm^{-1}$ = 2026s (CO), 1993w-sh (CO), 1840m (μ-CO), 1614m (μ-CN). IR (MeCN): $\tilde{\upsilon}/cm^{-1}$ = 2026s (CO), 1992w-sh (CO), 1839m (μ-CO), 1616m (μ-CN). No changes in the IR spectrum (*e.g.* related to CO/MeCN substitution) were observed after 44 h at room temperature. ^{1}H NMR (acetone-d_6): δ/ppm = 5.88, *5.83* (s, 10H, Cp); *4.19*, 4.15 (s, 6H, NCH_3); isomer (*cis*/*trans*) ratio ≈ 20; *ca*. 5% *trans* isomer in the final product, *ca*. 9 % before the final Et_2O washing. $^{13}C\{^1H\}$ NMR (acetone-d_6): δ/ppm = 295.4 (μ-CN); 231.0 (μ-CO); 197.6 (CO); *94.0*, 92.8 (Cp); 54.6 (NCH_3). ^{1}H NMR ($CDCl_3$): δ/ppm = 5.68, *5.59* (s, 10H, Cp); *4.13*, 4.06 (s, 6H, CH_3); isomer (*cis*/*trans*) ratio = 2.6 (incomplete dissolution, *trans* isomer is more soluble).

$[Ru_2Cp_2(CO)_2(\mu\text{-}CO)\{\mu\text{-}CNMe(Cy)\}]CF_3SO_3$, [2b]$CF_3SO_3$ (Chart 2).

Chart 2. Structure of [**2b**]$^+$ (numbering refers to C atoms).

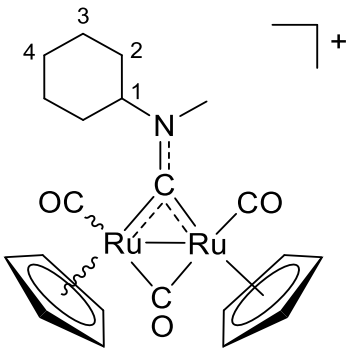

A yellow solution of [$Ru_2Cp_2(CO)_4$] (1.00 g, 2.25 mmol) in MeCN[96] (30 mL) was treated with cyclohexyl isocyanide (CNCy; 0.28 mL, 2.25 mmol) and stirred at room temperature for 69 h. The formation of [$Ru_2Cp_2(CO)_3$(CNCy)], **1b**, was checked by IR of the yellow solution (see ESI), then volatiles were removed under vacuum. The yellow residue was dissolved in CH_2Cl_2 (20 mL) and methyl triflate (1.8 mol/L in CH_2Cl_2; 1.12 mL, 2.02 mmol, 0.90 eq. *vs.* [$Ru_2Cp_2(CO)_4$]) was added dropwise, under vigorous stirring. The yellow solution was stirred at room temperature for 3 h, then moved on top of an alumina

column (h 4, d 5.4 cm). A yellow band containing unreacted $[Ru_2Cp_2(CO)_4]$ was eluted with CH_2Cl_2 then a yellow-orange band containing $[RuCpCl(CO)_2]$[50] was eluted with CH_2Cl_2/THF 4:1 *V*/*V*. Therefore, a bright yellow band containing [**2b**]$^+$ was eluted with MeCN and taken to dryness under vacuum. The residue was triturated in Et_2O/toluene 10:1 *V*/*V* and the suspension was filtered. The resulting yellow solid was washed with Et_2O and dried under vacuum (40 °C). Yield: 1.251 g, 86 %. The preparation was repeated four times on a 1-gram scale, always affording an 86 % yield of isolated product. Reduction of the reaction time of the first step to 24 h caused a slight lowering in the final yield. Soluble in EtOH, DMSO, CH_2Cl_2, less soluble in ^{i}PrOH, insoluble in Et_2O. X-ray quality crystals of [**2b**]CF_3SO_3 were obtained from a CH_2Cl_2 solution layered with Et_2O and settled aside at − 20 °C. Anal. calcd. for $C_{22}H_{24}F_3NO_6Ru_2S$: C, 38.32; H, 3.51; N, 2.03; S, 4.65. Found: C, 38.5; H, 3.63; N, 1.99; S, 4.60. IR (solid state): $\tilde{\upsilon}/cm^{-1}$ = 3110w, 2943w, 2931w-sh, 2098w, 2860w, 2010s (CO), 1983s (CO), 1951w-sh, 1823s (μ-CO), 1817w-sh, 1602w, 1573m (μ-CN), 1549w-sh, 1450w, 1430w, 1413w, 1403w, 1350w, 1321w, 1265s, 1257s (SO_3), 1225m-sh (SO_3), 1179w, 1147s (SO_3), 1057m, 1028s, 1012m, 997m, 992w, 893w, 876w, 850m, 837m, 830m, 824m, 798s, 749s. IR (CH_2Cl_2): $\tilde{\upsilon}/cm^{-1}$ = 2024s (CO), 1990w-sh (CO), 1841m (μ-CO), 1578w (μ-CN), 1552w. IR (MeCN): $\tilde{\upsilon}/cm^{-1}$ = 2024s (CO), 1989w-sh (CO), 1840m (μ-CO), 1580w (μ-CN). ^{1}H NMR ($CDCl_3$): δ/ppm = 5.71, *5.56* (s, 5H, Cp); 5.64, *5.49* (s, 5H, Cp'); 4.53-4.32 (m, 1H, C^{1}H); *4.01*, 3.84 (s, 3H, CH_3); 2.59, 2.10, 1.97 (d, $J \approx 12$ Hz, 3H, C^{2}H + C^{2}H); 1.90–1.73 (m, 4H, C$^{2'}$H + C^{4}H + C^{3}H), 1.44–1.24 (m, 3H, C^{3}H + C$^{3'}$H); isomer (*cis*/*trans*) ratio = 15, 6.3 % *trans* isomer. No changes were observed in the ^{1}H NMR spectrum after 14 h at room temperature. ^{13}C{^{1}H} NMR ($CDCl_3$): δ/ppm = 294.3 (μ-CN); 229.8 (μ-CO); 196.4, 195.7 (CO); 121.0 (d, $^1J_{CF}$ = 320 Hz, CF_3); *93.5*, *92.7*, 92.1, 91.8 (Cp + Cp'); 80.0 (C^1); *53.6*, 47.3 (CH_3); 31.3 (C^4), 30.4 (C^2), 26.1 (C^3), 26.0 (C$^{2'}$), 25.1 (C$^{3'}$). ^{19}F NMR ($CDCl_3$): δ/ppm = –78.2.

$[Ru_2Cp_2(CO)_2(\mu\text{-}CO)\{\mu\text{-}CNMe(Xyl)\}]CF_3SO_3$, [2c]$CF_3SO_3$ (Chart 3).

Chart 3. Structure of [**2c**]$^+$ (numbering refers to C atoms).

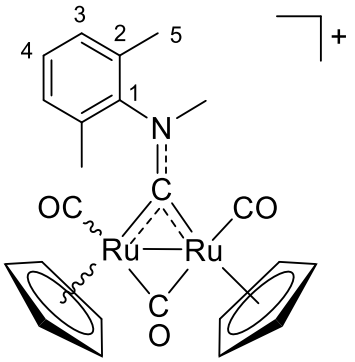

The title compound was previously reported but the synthetic procedure and IR/NMR data were not provided.[47] A yellow solution of $[Ru_2Cp_2(CO)_4]$ (200 mg, 0.45 mmol) in MeCN (12 mL) was treated with xylyl isocyanide (XylNC; 58 mg, 0.45 mmol) and stirred at room temperature (*ca*. 21 °C). After *ca*. 5 h, the formation of $[Ru_2Cp_2(CO)_3(CNXyl)]$, **1c**, was checked by IR of the yellow opalescent solution (ESI). After 24 h, a mixture of a yellow solution and a yellow solid was obtained. *Note*: IR analysis allowed to identify unreacted $[Ru_2Cp_2(CO)_4]$ in solution, while **1c** is undetectable due to massive precipitation. However, deceptive precipitation of yellow $[Ru_2Cp_2(CO)_4]$ occurred when operating with less solvent and/or at lower temperatures, resulting in zero CO/CNXyl exchange, even after prolonged times. The suspension was allowed to settle and the yellow solution, containing traces of $[Ru_2Cp_2(CO)_2(CNXyl)_2]$, was removed.[97] The yellow solid was washed once with MeCN (10 mL) and dried under vacuum. Next, the yellow residue was dissolved in CH_2Cl_2 (7 mL) and methyl triflate (1.8 mol/L in CH_2Cl_2; 0.15 mL, 0.27 mmol, 0.60 eq. *vs*. $[Ru_2Cp_2(CO)_4]$)[95] was added dropwise, under vigorous stirring. The resulting yellow solution was stirred at room temperature for 3 h, then moved on top of an alumina column (h 4, d 3.4 cm). A yellow band containing unreacted $[Ru_2Cp_2(CO)_4]$ was eluted with CH_2Cl_2 then a yellow-orange band containing $[RuCpCl(CO)_2]$[50] was eluted with THF. A bright yellow band containing [**2c**]$^+$ was eluted with MeCN and taken to dryness under vacuum. The residue was triturated in Et_2O and the suspension was filtered. The resulting yellow solid was washed with Et_2O and dried under vacuum (40 °C). Yield: 161 mg, 50 %. Soluble in EtOH, DMSO, CH_2Cl_2, MeCN;

insoluble in Et_2O. X-ray quality crystals of [**2c**]CF_3SO_3 were obtained from a CH_2Cl_2 solution layered with Et_2O and settled aside at − 20 °C. Anal. calcd. for $C_{24}H_{22}F_3NO_6Ru_2S$: C, 40.51; H, 3.12; N, 1.97; S, 4.51. Found: 40.29; H, 3.18; N, 1.98; S, 4.47. IR (solid state): $\tilde{\upsilon}/cm^{-1}$ = 3108w, 2017s (CO), 1988s-sh (CO), 1841s (μ-CO), 1591w, 1556m-sh, 1538m (μ-CN), 1469w, 1430w, 1414w, 1395w, 1386w, 1275s-sh, 1260s (SO_3), 1223m-sh (SO_3), 1149s (SO_3), 1115m, 1085w, 1061w, 1030s, 1014m-sh, 892w, 847m, 827m, 807m, 785s-sh, 774s, 755w-sh, 733m, 662m. IR (CH_2Cl_2): $\tilde{\upsilon}/cm^{-1}$ = 2027s (CO), 1994w-sh (CO), 1846m (μ-CO), 1593w, 1558w, 1540w (μ-CN). IR (MeCN): $\tilde{\upsilon}/cm^{-1}$ = 2026s (CO), 1993w-sh (CO), 1843m (μ-CO), 1594w, 1558w, 1543w (μ-CN). ^{1}H NMR ($CDCl_3$): δ/ppm = 7.34−7.19 (m, 3H*, C^3H + C^4H); 5.82, *5.30* (s, 5H, Cp); 5.23, *5.00* (s, 5H, Cp'); *4.37*, 4.21 (s, 3H, NCH_3); 2.53, *2.36*, *2.32*, 2.19 (s, 6H, C^5H_3); isomer (*cis*/*trans*) ratio ≈ *55*, *ca*. 2% *trans* isomer. *Over $CHCl_3$ peak. $^{13}C\{^1H\}$ NMR ($CDCl_3$): δ/ppm = 305.7 (μ-CN); 227.6 (μ-CO); 196.4, 195.9 (CO); 148.0 (C^1); 133.4, 131.5 (C^2); 129.9, 129.7, 129.5 (C^3 + C^4); 121.0 (d, $^1J_{CF}$ = 320 Hz, CF_3); 92.3, 91.6 (Cp + Cp'); 55.4 (NCH_3); 18.8, 17.7 (C^5). ^{19}F NMR ($CDCl_3$): δ/ppm = −78.2.

[Ru_2Cp_2(CO)(CNXyl)(μ-CO){μ-CNMe(Xyl)}]CF_3SO_3. Isolated by alumina chromatography; by-product of the synthesis of [**2c**]CF_3SO_3. IR (CH_2Cl_2): $\tilde{\upsilon}/cm^{-1}$ = 2113s (t-CN), 1988s (CO), 1824s (μ-CO), 1530m (μ-CN).

[$Ru_2Cp_2(CO)_2$(μ-CO){μ-CNMe(1*H*-indol-5-yl)}]CF_3SO_3, [2d]CF_3SO_3 (Chart 4).

Chart 4. Structure of [**2d**]$^+$ (numbering refers to C atoms).

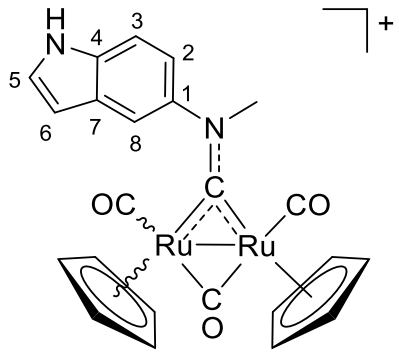

A yellow solution of $[Ru_2Cp_2(CO)_4]$ (150 mg, 0.34 mmol) in MeCN (12 mL) was treated with 1*H*-indol-5-yl isocyanide (IndNC; 53 mg, 0.37 mmol) and stirred at room temperature for 6 h, affording a yellow solution and a yellow solid. The formation of $[Ru_2Cp_2(CO)_3(CNInd)]$, **1d**, was checked by IR (ESI), then volatiles were removed under vacuum. The residue was dissolved in CH_2Cl_2 (8 mL) and methyl triflate (1.8 mol/L in CH_2Cl_2; 95 µL, 0.17 mmol, 0.50 eq. *vs*. $[Ru_2Cp_2(CO)_4]$) was added dropwise, under vigorous stirring. The yellow solution was stirred at room temperature for 3 h. The resulting suspension (yellow solution + yellow solid) was moved on top of an alumina column (h 4, d 3.4 cm). A yellow band containing unreacted $[Ru_2Cp_2(CO)_4]$ was eluted with CH_2Cl_2 then a yellow-orange band containing $[RuCpCl(CO)_2]$[50] was eluted with THF. A bright yellow band containing $[\mathbf{2d}]^+$ was eluted with MeCN and taken to dryness under vacuum. The residue was triturated in Et_2O/toluene 10:1 *V*/*V* and the suspension was filtered. The resulting yellow solid was washed with Et_2O and dried under vacuum (40 °C). Yield: 53 mg, 23 %. Increasing reaction time (> 20 h) or temperature (reflux) during the first step causes darkening of the reaction mixture and a significant drop in aminocarbyne yield. Soluble in EtOH, DMSO, acetone, less soluble in CH_2Cl_2, $CHCl_3$, insoluble in Et_2O. X-ray quality crystals of $[\mathbf{2d}]CF_3SO_3$ were obtained from a CH_2Cl_2 solution layered with toluene and settled aside at − 20 °C. Anal. calcd. for $C_{24}H_{19}F_3N_2O_6Ru_2S$: C, 39.89; H, 2.65; N, 3.88; S, 4.44. Found: C, 40.28; H, 2.63; N, 4.05; S, 4.26. IR (solid state): $\tilde{\upsilon}/cm^{-1}$ = 3226w, 3106w, 2011s (CO), 1990s-sh (CO), 1840s (µ-CO), 1587w, 1562m, 1548m-sh (µ-CN), 1477w, 1460w, 1430w, 1415w, 1399w, 1346w, 1324w, 1280s, 1269s, 1246s (SO_3), 1224s-sh (SO_3), 1157s (SO_3), 1108m, 1066w, 1029s, 999w-sh, 895w, 874w, 844m, 835m, 814m, 799m, 773s, 742m, 730m. IR (CH_2Cl_2): $\tilde{\upsilon}/cm^{-1}$ = 2025s (CO), 1995m-sh (CO), 1841m (µ-CO), 1584w, 1561w, 1548w (µ-CN). IR (MeCN): $\tilde{\upsilon}/cm^{-1}$ = 2026s (CO), 1992w-sh (CO), 1840m (µ-CO). ^{1}H NMR (acetone-d_6): δ/ppm = 10.8 (s, 1H, NH); *7.95*, 7.91 (d, $^4J_{HH} \approx 1$ Hz, C^{8}H); 7.71 (d, $^3J_{HH}$ = 8.6 Hz, C^{3}H); 7.62–7.54 (m, C^{5}H); *7.44*, 7.41 (dd, $^3J_{HH}$ = 8.6 Hz, $^4J_{HH} \approx 1$ Hz, 1H, C^{2}H); 6.66–6.61, *6.58–6.56* (m, 1H, C^{6}H); 5.99, *5.96* (s, 5H, Cp); 5.28, *5.18* (s, 5H, Cp'); *4.62*, 4.53 (s, 3H, CH_3); isomer (*cis*/*trans*) ratio ≈ 13; *ca*.

7% *trans* isomer. $^{13}C\{^{1}H\}$ NMR (acetone-d_6): δ/ppm = 302.0 (μ-CN); 230.4 (μ-CN); 198.3, 197.7 (CO); 144.3 (C^1); 136.5 (C^4); 129.1 (C^7); 128.7 (C^5); 118.7 (C^2); 117.3 (C^8); 113.5 (C^3); 103.3 (C^6); *94.1*, 93.1 (Cp); *93.8*, 92.7 (Cp'); 58.1 (CH_3). ^{19}F NMR (acetone-d_6): δ/ppm = − 78.7.

Alternative procedure: Me_3NO-assisted isocyanide coordination.

Preliminary note: the $[Ru_2Cp_2(CO)_4]$/isocyanide/Me_3NO system revealed highly sensitive to the reaction conditions (solvent/temperature, reactant excess and addition order). The following procedure was optimized based on the reactivity with 2-naphthyl isocyanide and benzyl isocyanide.

General procedure: A solution of $[Ru_2Cp_2(CO)_4]$ (100 mg, 0.23 mmol) in THF (5 mL) was treated with the selected isocyanide (0.7 or 1.0 eq.) and Me_3NO (2.3 or 4.0 eq.), in this order, and rapidly placed on a pre-heated oil bath. The mixture was heated at reflux temperature under stirring for 3 h. The resulting dark solution was analysed by IR (see ESI). Very poor or negligible formation of $[Ru_2Cp_2(CO)_3(CNR)]$ was observed with diethyl isocyanomethylphosphonate, 4-ethylphenyl isocyanide and *p*-toluenesulfonylmethyl isocyanide, even after prolonged heating (up to 16 h). A modest yield of $[Ru_2Cp_2(CO)_3(CNR)]$ (**1e-g**) was observed with 2-naphthyl isocyanide, 4-methoxyphenyl isocyanide and α-(*S*)-methylbenzyl isocyanide, as checked by IR (ESI).[98] In these cases, the mixture was allowed to cool to room temperature and volatiles were removed under vacuum. The residue was dissolved in CH_2Cl_2 (5 mL) and methyl triflate (1.8 mol/L in CH_2Cl_2; 0.12 mL, 0.22 mmol) was added dropwise, under vigorous stirring. The solution was stirred at room temperature for 3 h, then moved on top of an alumina column (h 4, d 2.4 cm). A yellow band containing unreacted $[Ru_2Cp_2(CO)_4]$ was eluted with CH_2Cl_2 then a yellow-orange band containing $[RuCpCl(CO)_2]$[50] and other impurities was eluted with CH_2Cl_2/THF 1:1 *V*/*V*. A band containing the desired aminocarbyne complex $[$**2e-g**$]^+$ was eluted with MeCN or THF/MeCN 7:1 *V*/*V* and taken to dryness under vacuum. The resulting yellow-brown solid was washed with Et_2O, hexane and dried under vacuum (40 °C).

[$Ru_2Cp_2(CO)_2(\mu\text{-}CO)\{\mu\text{-}CNMe(2\text{-naphthyl})\}]CF_3SO_3$, [2e]$CF_3SO_3$ (Chart 5).

Chart 5. Structure of [**2e**]$^+$.

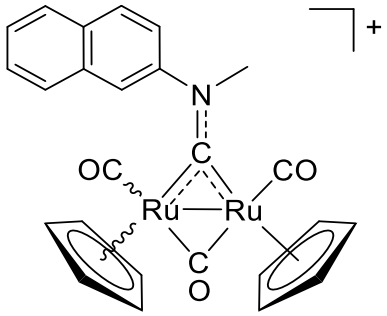

Prepared using 2-naphthyl isocyanide (35 mg, 0.23 mmol) and Me_3NO (68 mg, 0.90 mmol), according to the general procedure. Only minor signals ascribable to by-products are present in the isolated material (^{1}H NMR). Yield: 41 mg, *ca.* 23 %. A comparable result was obtained when using $Me_3NO{\cdot}2H_2O$ in place of anhydrous Me_3NO. IR (CH_2Cl_2): $\tilde{\upsilon}/cm^{-1}$ = 2026s (CO), 1993m-sh (CO), 1842m (μ-CO), 1582w, 1576w, 1554w, 1544w (μ-CN). ^{1}H NMR ($CDCl_3$): δ/ppm = 8.38 (s-br, 1H), 8.10–8.03 (m, 2H), 7.96–7.88 (m, 1H), 7.70 (s-br, 1H), 7.67–7.59 (m, 2H), ($C_{10}H_7$); 5.82, *5.74* (s, 5H, Cp), 5.10, *4.95* (s, 5H, Cp'); *4.61*, 4.45 (s, 3H, CH_3); isomer (*cis*/*trans*) ratio ≈ 25, *ca*. 4% *trans* isomer in the final product, *ca*. 8 % before the final Et_2O washing.

[$Ru_2Cp_2(CO)_2(\mu\text{-}CO)\{\mu\text{-}CNMe(4\text{-}C_6H_4OMe)\}]CF_3SO_3$, [2f]$CF_3SO_3$ (Chart 6).

Chart 6. Structure of [**2f**]$^+$.

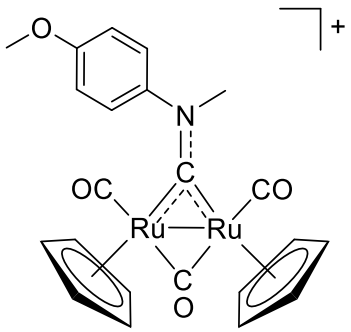

Prepared using 4-methoxyphenyl isocyanide (20 mg, 0.15 mmol) and Me_3NO (40 mg, 0.53 mmol), according to the general procedure. The solid contains minor {RuCp} by-products (*ca*. 25 % overall), as detected by ^1H NMR, which prevent an unambiguous identification of signals ascribable to the *trans* isomer. IR (CH_2Cl_2): $\tilde{\upsilon}/cm^{-1}$ = 2025s (CO), 1991m-sh (CO), 1841m (μ-CO), 1607w, 1571w, 1550w (μ-CN). ^1H NMR ($CDCl_3$): δ/ppm = 7.64 (d, $^3J_{HH}$ = 8.1 Hz, 2H, C_6H_{ortho}); 7.07 (d, $^3J_{HH}$ = 9.0 Hz, 2H, C_6H_{meta}); 5.78 (s, 5H, Cp); 5.21 (s, 5H, Cp'); 4.34 (s, 3H, NCH_3); 3.89 (s, 3H, OCH_3).

[$Ru_2Cp_2(CO)_2$(μ-CO){μ-(*S*)-CN(Me)CH(Me)Ph)}]CF_3SO_3, [2g]CF_3SO_3 (Chart 7).

Chart 7. Structure of [**2g**]$^+$.

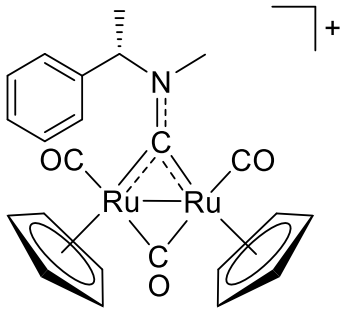

Prepared using (*S*)-α-methylbenzyl isocyanide (31 μL, 0.23 mmol) and Me_3NO (68 mg, 0.90 mmol) according to the general procedure. The solid contains minor {RuCp} by-products (*ca*. 15 % overall), as detected by ^1H NMR, which prevent an unambiguous identification of signals ascribable to the *trans* isomer. X-ray quality crystals of [**2g**]CF_3SO_3 were obtained from a CH_2Cl_2 solution layered with Et_2O and settled aside at − 20 °C. IR (CH_2Cl_2): $\tilde{\upsilon}/cm^{-1}$ = 2025s (CO), 1992m-sh (CO), 1843m (μ-CO), 1573w, 1563w (μ-CN). ^1H NMR ($CDCl_3$): δ/ppm = 7.68−7.30 (m, Ph); 5.99−5.89 (m, 1H, NCH); 5.76, 5.73 (s, 5H, Cp); 5.70, 5.66 (s, 5H, Cp'); 3.66, 3.56 (s, 3H, NCH_3); 2.12, 1.83 (d, $^3J_{HH}$ = 7.1 Hz, 3H, CCH_3).

4.2.1. Thermal isomerization studies

In a round bottom flask, a yellow solution of the selected Ru compound (10 mg) in ^{i}PrOH (10 mL) was heated at reflux for 1.5-5 h. Volatiles were removed under vacuum and the residue was analysed by ^1H

NMR to assess the % of *trans* isomer with respect to the starting material (s.m. in the following). [**2a**]$^+$ (acetone-d_6): 9 % (s.m.), *ca*. 5 % (1.5 h). [**2b**]$^+$ ($CDCl_3$): 6.3 % (s.m.), *ca*. 1 % (3 h). [**2e**]$^+$ ($CDCl_3$): 8 % (s.m.), *ca*. 4 % (5 h).

4.3. X-ray crystallography

Crystal data and collection details for [**2a-d,g**]CF_3SO_3 are reported in Tables S4-S5. Data were recorded on a Bruker APEX II diffractometer equipped with a PHOTON2 detector using Mo–Kα radiation. Data were corrected for Lorentz polarization and absorption effects (empirical absorption correction SADABS).[99] The structures were solved by direct methods and refined by full-matrix least-squares based on all data using F^2.[100] Hydrogen atoms were fixed at calculated positions and refined by a riding model. All non-hydrogen atoms were refined with anisotropic displacement parameters.

4.4. Solubility and stability in aqueous solutions, octanol-water partition coefficient

Solubility in water (D_2O). The selected compound was suspended in a D_2O solution (0.7 mL) containing dimethyl sulfone (Me_2SO_2; $4.0 \cdot 10^{-3}$ mol/L) and stirred at room temperature (*ca.* 21 °C) for 3 h. The saturated solution was filtered over celite and analysed by ^{1}H NMR spectroscopy (delay time = 3 s, number of scans = 20). The concentration (= solubility) was calculated by the relative integral with respect to Me_2SO_2 as internal standard [δ/ppm = 3.14 (s, 6H)] (Table 2). NMR data are reported in the Supporting Information.

Octanol-water partition coefficient (Log P_{ow}). Partition coefficients (P_{ow}), defined as $P_{ow} = c_{org}/c_{aq}$, where c_{org} and c_{aq} are the molar concentrations of the selected compound in the n-octanol and aqueous phases, respectively, were determined by the shake-flask method and UV-Vis measurements, according to a previously described procedure.[30,101] All operations were carried out at room temperature (*ca*. 21 °C). Stock solutions were prepared in water-saturated octanol for all compounds except [**2a**]CF_3SO_3 (in

octanol-saturated water). The wavelength corresponding to a well-defined maximum of shoulder absorption of each compound (320–400 nm range) was used for UV-Vis quantitation. The procedure was repeated three times for each sample (from the same stock solution); results are given as mean ± standard deviation (Table 2).

Stability assessment in D_2O/CD_3OD at 37 °C. The selected compound was dissolved in CD_3OD (0.3 mL) then diluted with a D_2O solution containing Me_2SO_2 ($4.0 \cdot 10^{-3}$ mol/L, 0.5 mL). The yellow solution ($c_{Ru2} \approx 8 \cdot 10^{-3}$ mol/L; D_2O/CD_3OD 5:3 *V*/*V*)[102] was filtered over celite and analysed by ^1H NMR (delay time = 3 s; number of scans = 20). Next, the solution was heated at 37 °C for 72 h and NMR analyses were repeated. The residual amount of starting material in the final solution, calculated by the relative integral with the internal standard (Me_2SO_2) with respect to the initial spectrum, resulted ≥ 99 % for all compound tested ([**2a-e,h**]CF_3SO_3). NMR data are reported in the ESI. ^1H NMR chemical shifts in D_2O/CD_3OD mixtures are referenced to the Me_2SO_2 peak in pure D_2O [δ/ppm = 3.14 (s, 6H)]. The % amount of *trans* isomers is in accordance with that observed in $CDCl_3$ or acetone-d_6 solutions; besides, no change in the *cis*/*trans* ratio was observed over the course of the experiment.

Stability assessment in cell culture medium at 37 °C. Deuterated cell culture medium (DMEM-d) was prepared by dissolving powdered DMEM cell culture medium (1000 mg/L glucose and L-glutamine, without sodium bicarbonate and phenol red; D2902 - Sigma Aldrich) in D_2O (10 mg/mL, according to the manufacturer's instructions). The solution was treated with Me_2SO_2 ($8.3 \cdot 10^{-3}$ mol/L) and KH_2PO_4 / Na_2HPO_4 as pH buffer (0.10 mol/L total phosphate, pD = 7.4[103]), then stored at 4 °C under N_2. Solutions of Ru compounds in DMEM-d/CD_3OD 5:3 *V*/*V* were prepared, treated and analysed by ^1H NMR as previously described. The residual amount of starting material in the final solution resulted ≥ 99 % for all compound tested ([**2a-d**]CF_3SO_3). No change in *cis*/*trans* ratios was observed.

4.5. Electrochemistry

Cyclic voltammetry measurements were performed with a PalmSens4 instrument interfaced to a computer employing PSTrace5 electrochemical software. All potentials are reported *vs.* Ag/AgCl/KCl. Peak potentials for compounds [**2b,c**]CF_3SO_3 are compiled in Table 3, cyclic voltammograms are given in Figures S31-S32.

Experiments in dichloromethane. HPLC grade dichloromethane (Sigma Aldrich) was stored under Ar over 3Å MS. [^{n}Bu$_4$N][PF_6] (Fluka, electrochemical grade) and Cp_2Fe (Fluka) were used without further purification. CV measurements were carried out at room temperature under Ar using 0.2 mol/L [^{n}Bu$_4$N][PF_6] in CH_2Cl_2 as the supporting electrolyte. The working and the counter electrode consisted of a Pt disk and a Pt gauze, respectively. A leakless miniature Ag/AgCl/KCl electrode (eDAQ) was employed as a reference. The three-electrode home-built cell was pre-dried by heating under vacuum and filled with argon. The Schlenk-type construction of the cell maintained anhydrous and anaerobic conditions. The solution of supporting electrolyte, prepared under argon, was introduced into the cell and the CV of the solvent was recorded. The analyte was then introduced ($c \approx 1 \cdot 10^{-3}$ mol/L) and voltammograms were repeated (scan rate: 0.1 V/s); then a small amount of ferrocene was added and the voltammograms repeated. Under the present experimental conditions, the one-electron reduction of ferrocene occurred at $E° = +0.45$ V vs. Ag/AgCl/KCl.

Experiments in aqueous media. Phosphate buffer (PB) solution (Na_2HPO_4/KH_2PO_4, $\Sigma c_{(PO4)}$ = 25 mmol/L, pH = 7.3) prepared in ultrapure H_2O was used as supporting electrolyte. The three-electrode home-built cell was equipped with a Pt sheet counter electrode, teflon-encapsulated glassy-carbon (GC) working electrode (BASi, ø 3 mm) and the leak-free Ag/AgCl/KCl reference electrode (eDAQ). Prior to measurements, the working GC electrode was polished by the following procedure:[104] manual rubbing with 0.3 μM Al_2O_3 slurry in water (eDAQ) for 2 min, then sonication in ultrapure water for 10 min, manual rubbing with 0.05 μM Al_2O_3 slurry in water (eDAQ) for 2 min, then sonication in ultrapure water for 10 min. The supporting electrolyte (5.0 mL) was introduced into the cell, deareated by Ar bubbling

for some minutes and the CV of the solvent was recorded. The analyte was then introduced (c ≈ 0.7-1.0·10^{-3} mol/L) and voltammograms were recorded (scan rate: 0.1 V/s).

4.6. Interactions with GSH and bovine serum albumin

Methanol solutions of selected complexes, i.e. [**2a**]CF_3SO_3 and [**2d**]CF_3SO_3, were mixed with a solution of GSH in water to generate a system containing a 10 μM concentration of the complexes and a 10 mM concentration of GSH. Mass spectra of the reacting systems were acquired using a Shimadzu LC-MS 8050 Liquid Chromatograph Mass Spectrometer with electrospray ionization source in positive ionization mode. The spectra of [**2a**]CF_3SO_3 and [**2d**]CF_3SO_3 in methanol were obtained using the Bruker amaZon SL mass spectrometer with the same electrospray ionization setup. The collected data were analysed using dedicated software (Bruker, Data Analysis 4.4; Shimadzu, LabSolutions Connect software).

The interaction studies of [**2a**]CF_3SO_3 and [**2d**]CF_3SO_3 with bovine serum albumin were performed using the same method as reported previously.[41] In brief, bovine serum albumin (BSA, 30 μM in 50 mM NH_4HCO_3) was incubated with the selected complexes ([**2a**]CF_3SO_3 and [**2d**]CF_3SO_3, 1 mM) at 37 °C for 48h. The resulting solutions underwent processing for MALDI-TOF MS analysis using the sinapinic acid matrix. Mass spectra were collected using a Microflex LRF20 MALDI-TOF mass spectrometer and analysed with flexAnalysis 3.4 software (Bruker Daltonik).

4.7. Biological studies

Cell viability assay (MTT test). For the evaluation of in vitro cytotoxicity, the human cancer cell lines A2780, A2780R, MCF-7, HOS, A549, PANC1, CaCo2, PC3 and HeLa, as well as normal fetal lung fibroblasts (MRC-5), were selected. The cells were plated in 96-well dishes, using culture media supplemented with 10% fetal calf serum, following the conditions recommended by the supplier. Stock solutions of the complexes were prepared immediately before cell treatment in DMF and further diluted

with culture media to achieve final concentrations of the tested complexes (at levels of 0.1, 1, 10, 25 and 50 μM containing 0.1% *V*/*V* DMF) for a 24h treatment. The negative control consisted of vehicle-treated cells (0.1% *V*/*V* DMF) and the positive control comprised Triton X-100 treated cells (1%; *V*/*V* in culture media) for 24 h. The MTT assay was conducted, and absorbance (A) was measured spectrophotometrically at 570 nm using an Infinite M200 instrument (Schoeller Instruments, Prague, Czech Republic). The data were expressed as the percentage of cell viability, where 100% and 0% represent treatments with the negative control (DMF) and positive control (Triton X-100), respectively. Half-maximal inhibitory concentrations (IC_{50}) were calculated using GraphPad Prism 6 software (GraphPad Software, San Diego, USA).

Cell culture. The human ovarian cancer cell line A2780 (Sigma, 93112519-1VL) was employed for further experiments investigating the cellular effects of the selected complexes, [**2a**]CF_3SO_3 (at 50 μM concentration) and [**2d**]CF_3SO_3 (at 3.7 μM concentration). In all experiments, the reference drug cisplatin (15 μM) and a vehicle (0.1 % DMF), serving as a negative control, were included. Cells were incubated at 37 °C under a 5% CO_2 atmosphere in complete RPMI-1640 Medium (Merck, USA) with final concentrations of L-Glutamine (2 mM), fetal bovine serum (FBS, 10%), penicillin (5 U/mL) and streptomycin (50 μg/mL).

Cell cycle analysis. To investigate changes in the cell cycle, 10^4 cells/well were seeded in a 96-well plate. The following day, cells were treated with 50 μM of [**2a**]CF_3SO_3 or 3.7 μM of [**2d**]CF_3SO_3 and incubated for 24h. Then, the supernatant was discarded, and samples were washed once with PBS (0.1M, pH 7.4). Flow cytometry analysis was performed using a BD FACSVerse flow cytometer (Becton Dickinson, USA) with the BD Cycletest^{TM} Plus DNA kit (Becton Dickinson, USA), following the manufacturer's protocol. Measurements were conducted in duplicates and at least $5{\cdot}10^3$ events were recorded for each sample. The reference drug cisplatin was also as a positive control for this assay.

Apoptosis analysis. The impact of the selected complexes on the apoptosis of A2780 cells was investigated using two different assays: the Annexin V-FITC apoptosis detection kit (Enzo Life Sciences,

USA) and the CellEvent™ Caspase-3/7 Green Flow Cytometry Assay Kit (Thermo Fisher Scientific, USA) for the assessment of caspase induction. The experiments were performed following the manufacturers' protocols, with the CellEventTM Caspase-3/7 Green Detection Reagent used specifically for detecting Caspase-3/7 activation. Briefly, A2780 cells were seeded in 24-well plate at $50 \cdot 10^3$ cells/well and treated the next day with 50 µM of [**2a**]CF_3SO_3 and 3.7 µM of [**2d**]CF_3SO_3 for 24 h. After incubation, the supernatant was collected, cells were washed once with PBS (0.1M, pH 7.4), detached with trypsin (0.25% in ethylenediaminetetraacetic acid - EDTA, Merck), resuspended in 500 µL of culture medium and collected into Eppendorf tubes. The samples were stained with specific dyes and incubated following the protocols (10 min in the dark at room temperature for Annexin V-FITC/PI and 30 min in the incubator at 37 °C for the CellEventTM Caspase-3/7 Green Detection Reagent). Finally, measurements were performed with a BD FACSVerse flow cytometer (Becton Dickinson, USA) in duplicates, and at least 10^4 events were recorded for each sample. For positive controls, the reference drug cisplatin was used for Apoptosis, while heat-damaged cells (10 min at 60 °C) were used for caspase activation.

Autophagy analysis. CYTO-ID® Autophagy Detection Kit 2.0 (Enzo Life Sciences, USA) was employed for assessing the potential autophagy induction in A2780 cells caused by the selected complexes. Briefly, cells were seeded in a 24-well plate ($50 \cdot 10^3$ cells/well) and treated the following day for 24 h with selected concentrations of [**2a**]CF_3SO_3 (50 µM) and [**2d**]CF_3SO_3 (3.7 µM). After incubation with the complexes, supernatants were collected, cells were washed with warm PBS, detached using 0.25% trypsin-EDTA (Gibco™), resuspended in a cell culture medium and collected into Eppendorf tubes. Staining of the samples was performed using the specific dye (Diluted CYTO-ID® Green stain solution) according to the manufacturer's protocol. Samples were incubated in the dark for 30 minutes at room temperature. Subsequently, after one washing with warm PBS, flow cytometry analysis was conducted using a BD FACSVerse flow cytometer (Becton Dickinson, USA). Samples were run in

duplicates, with at least 10^4 events recorded/sample. As a positive control, cells were treated with a mixture of chloroquine (10 µM) and rapamycin (0.5 µM) for 24 hours.

Oxidative stress analysis. For the analysis of oxidative stress, the total ROS production in cells treated with 50 µM of [**2a**]CF_3SO_3 and 3.7 µM of [**2d**]CF_3SO_3 was determined using the ROS-ID® Total ROS/Superoxide detection kit (Enzo Life Sciences, US). The measurement was performed according to the manufacturer's protocol, and a 100 µM solution of pyocyanin, a known oxidative-stress inducer, was used as a positive control. Briefly, after seeding the cells in a 96-well plate (10^4 cells/well), they were exposed to the tested compounds for 24 h. Then, supernatants were removed, cells were washed with wash buffer (1X) and staining was performed for 60 min at 37 °C in the dark, using the ROS/Superoxide Detection Solution (prepared according to the protocol). The fluorescence (Ex. 488 nm/Em. 520 nm) of samples was then analysed in triplicates with a microplate reader Infinite M200Pro (Tecan, Switzerland).

Mitochondrial membrane potential (MMP) analysis. The effect on the mitochondrial membrane potential was studied using the MITO-ID® Membrane potential detection kit (Enzo Life Sciences, USA). After seeding A2780 cells (5×10^4 cells/well) in a 24-well plate, treatment with selected concentrations of [**2a**]CF_3SO_3 (50 µM) and of [**2d**]CF_3SO_3 (3.7 µM) was applied for 24 h. Then, following supernatant collection, cell washing with PBS, detachment of cells, and resuspension in the cell culture medium, samples were incubated for 15 min at room temperature with MITO-ID® MP Detection Reagent (according to the protocol). Finally, at least 10^4 events were recorded in duplicates for each sample using a BD FACSVerse flow cytometer (Becton Dickinson, USA). A positive control, 2 µM carbonyl cyanide 3-chlorophenylhydrazone (CCCP), was utilized.

Statistical analysis. Biological experiments were conducted in triplicate (three independent experiments) and the results are presented as the mean ± standard deviation (SD). One-way ANOVA was performed using Statistica software to assess the significance of difference between samples. Statistically significant differences at $p \leq 0.05$ have been denoted by different letters.

Cellular uptake. Solutions of the selected complexes, [**2a**]CF_3SO_3 (final conc. 50 μM), [**2d**]CF_3SO_3 (final conc. 3.7 μM), and RAPTA-C (final conc. 50 μM), were added to A2780 cells (between 6th and 15th passage). The cells were then incubated at 37 °C under a 5% CO_2 atmosphere in complete RPMI-1640 Medium (Merck, USA). The medium was supplemented with L-Glutamine, fetal bovine serum, 5 U/mL penicillin and 50 μg/mL streptomycin for different time points: 2, 6, 12, 24, 48, and 72 h. Following the respective incubation periods, adherent cells were detached, suspended, washed with PBS, and concentrated by centrifugation. Supernatants were discarded, and the resulting cell pellets were digested with 500 μL of nitric acid (for ICP-MS, 65%, overnight). Afterwards, solutions were diluted with 4.5 mL of ultrapure water for trace analysis, and the ruthenium (Ru) content was determined by ICP-MS (ICP-MS spectrometer 7700x, Agilent) using external calibration. The obtained values were corrected for adsorption effects.

Conflicts of interest. The authors declare no competing financial interest.

Acknowledgements. L.B., T.F. and F.M. thank the University of Pisa (Fondi di Ateneo 2020 and PRA_2020_39) for financial support. J.V., T.M. and Z.T. acknowledge the financial support from ERDF/ESF project Nanotechnologies for Future (CZ.02.1.01/0.0/0.0/16_019/0000754) and thank to Ms. Marta Rešová for help with biological testing, Prof. Marek Šebela for assistance with MALDI-TOF MS experiments, and Dr. Ondřej Vrobel for assistance with some of the mass spectrometry experiments.

Supplementary material. IR and NMR spectra of diruthenium aminocarbyne complexes in organic solvents and aqueous solution. Synthesis and characterization of [**3a**]CF_3SO_3. Comparison of NMR, IR, Log P_{ow} data for homologous diiron and diruthenium isocyanide and aminocarbyne complexes. Cyclic voltammograms. X-ray crystallography data. CCDC reference number 2320423 ([**2a**]CF_3SO_3), 2320424 ([**2b**]CF_3SO_3), 2320425 ([**2c**]CF_3SO_3), 2320426 ([**2d**]CF_3SO_3) and 2320427 ([**2g**]CF_3SO_3) contain the

supplementary crystallographic data for the X-ray studies reported in this paper. These data can be obtained free of charge at https://www.ccdc.cam.ac.uk/structures (or from the Cambridge Crystallographic Data Centre, 12, Union Road, Cambridge CB2 1EZ, UK; fax: (internat.) +44-1223/336-033; e-mail: deposit@ccdc.cam.ac.uk).

References

1 M. Marloye, G. Berger, M. Gelbcke, A survey of the mechanisms of action of anticancer transition metal complexes. Future Med. Chem. 2016, 8, 2263-2286.

2 E. Boros, P. J. Dyson, G. Gasser, Classification of Metal-Based Drugs according to Their Mechanisms of Action. Chem 2020, 6, 41–60.

3 B. S. Murray, P. J. Dyson, Recent progress in the development of organometallics for the treatment of cancer. Curr. Opinion Chem. Biol. 2020, 56, 28-34.

4 Anthony, E. J.; Bolitho, E. M.; Bridgewater, H. E.; Carter, O. W. L.; Donnelly, J. M.; Imberti, C.; Lant, E. C.; Lermyte, F.; Needham, R. J.; Palau, M.; Sadler, P. J.; Shi, H.; Wang, F.-X.; Zhang, W.-Y.; Zhang, Z. Metallodrugs are unique: opportunities and challenges of discovery and development. Chem. Sci. 2020, 11, 12888–12917.

5 G. Gasser, N. Metzler-Nolte, The potential of organometallic complexes in medicinal chemistry, Curr. Opinion Chem. Biol. 2012, 16, 84–91.

6 A. Kondratskyi,, K. Kondratska, F. Vanden Abeele, D. Gordienko, C. Dubois, R.-A. Toillon, C. Slomianny, S. Lemière, P. Delcourt, E. Dewailly, R. Skryma, C. Biot, N. Prevarskaya, Ferroquine, the next generation antimalarial drug, has antitumor activity, Sci. Reports 2017, 7, 15896.

7 W. A. Wani, E. Jameel, U. Baig, S. Mumtazuddin, L. Ting Hun, Ferroquine and its derivatives: New generation of antimalarial agents, Eur. J. Med. Chem. 2015, 101, 534e551.

8 Murray, B. S.; Babak, M. V.; Hartinger, C. G.; Dyson, P. J. The development of RAPTA compounds for the treatment of tumors, Coord. Chem. Rev. 2016, 306, 86–114.

9 Steel, T. R.; Walsh, F.; Wieczorek-Błauz, A.; Hanif, M.; Hartinger, C. G. Monodentately-coordinated bioactive moieties in multimodal half-sandwich organoruthenium anticancer agents, Coord. Chem. Rev. 2021, 439, 213890.

10 P. J. Dyson, Ruthenium – A Non-essential Element that May Become Essential in Treating Chemoresistant Cancers, Chimia 2019, 73, 332–333.

11 Alessio, E. Thirty years of the drug candidate NAMI-A and the myths in the field of ruthenium anticancer compounds: A personal perspective. Eur. J. Inorg. Chem. 2017, 2017, 1549 − 1560.

12 Rausch, M.; Dyson, P. J.; Nowak-Sliwinska, P. Recent Considerations in the Application of RAPTA-C for Cancer Treatment and Perspectives for Its Combination with Immunotherapies, Adv. Therap. 2019, 2, 1900042.

13 Weiss, A.; Berndsen, R. H.; Dubois, M.; Müller, C.; Schibli, R.; Griffioen, A. W.; Dyson, P. J.; Nowak-Sliwinska, P. In vivo anti-tumor activity of the organometallic ruthenium(II)-arene complex [Ru(η^6-p-cymene)-Cl_2(pta)] (RAPTA-C) in human ovarian and colorectal carcinomas. Chem. Sci., 2014, 5 , 4742–4748.

14 T. Ranjan Panda, M. M, Shreyas P. Vaidya, S. Chhatar, S. Sinha, M. Mehrotra, S. Chakraborty, S. Gadre, P. Duari, P. Ray, M. Patra, The Power of Kinetic Inertness in Improving Platinum Anticancer Therapy by Circumventing Resistance and Ameliorating Nephrotoxicity, Angew. Chem. Int. Ed. 2023, 62, e202303958.

15 S. Parveen, M. Hanif, S. Movassaghi, M. P. Sullivan, M. Kubanik, M. A. Shaheen, T. Söhnel, S. M. F. Jamieson, C. G. Hartinger, Cationic Ru(η^6-p-cymene) Complexes of 3-Hydroxy-4-pyr(id)ones– Lipophilic Triphenylphosphine as Co-Ligand Is Key to HighlyStable and Cytotoxic Anticancer Agents, Eur. J. Inorg. Chem. 2017, 1721–1727.

16 S. Banerjee, J. J. Soldevila-Barreda, J. A. Wolny, C. A. Wootton, A. Habtemariam, I. Romero-Canelon, F. Chen, G. J. Clarkson, I.Prokes, L. Song, P. B. O'Connor, V. Schünemann, P. J. Sadler, New activation mechanism for half-sandwich organometallic anticancer complexes, Chem. Sci., 2018, 9, 3177–3185.

17 Z. Adhireksan, G. E. Davey, P. Campomanes, M. Groessl, C. M. Clavel, H. Yu, A. A. Nazarov, C. H. Fang Yeo, W. H. Ang, P. Droge, U. Rothlisberger, P. J. Dyson, C. A. Davey, Ligand substitutions between ruthenium–cymene compounds can control protein versus DNA targeting and anticancer activity, Nat. Commun. 2014, 5, 3462.

18 S. Keller, Y. Ching Ong, Y. Lin, K. Cariou, G. Gasser, A tutorial for the assessment of the stability of organometallic complexes in biological media, J. Organomet. Chem. 2020, 906, 121059.

19 M. D. Hall, K. A. Telma, K.-E. Chang, T. D. Lee, J. P. Madigan, J. R. Lloyd, I. S. Goldlust, J. D. Hoeschele, M. M. Gottesman, Say No to DMSO: Dimethylsulfoxide Inactivates Cisplatin, Carboplatin, and Other Platinum Complexes, Cancer Res. 2014, 74, 3913-3922.

20 S. Swaminathan, J. Haribabu, N. Balakrishnan, P. Vasanthakumar, R. Karvembu, Piano stool Ru(II)-arene complexes having three monodentate legs: A comprehensive review on their development as anticancer therapeutics over the past decade, Coord. Chem. Rev. 2022, 459, 214403.

21 L. Biancalana, G. Pampaloni, S. Zacchini, F. Marchetti, Synthesis, characterization and behavior in water/DMSO solution of Ru(II) arene complexes with bioactive carboxylates, J. Organomet. Chem. 2018, 869, 201-211.

22 V. Ritleng, M. J. Chetcuti, Hydrocarbyl Ligand Transformations on Heterobimetallic Complexes, Chem. Rev. 2007, 107, 797−858.

23 F. Marchetti, Constructing Organometallic Architectures from Aminoalkylidyne Diiron Complexes. Eur. J. Inorg. Chem. 2018, 3987–4003.

24 G. Bresciani, S. Schoch, L. Biancalana, S. Zacchini, M. Bortoluzzi, G. Pampaloni, F. Marchetti, Cyanide–alkene competition in a diiron complex and isolation of a multisite (cyano)alkylidene–alkene species. Dalton Trans. 2022, 51, 1936-1945.

25 S. Patra, N. Maity, Recent advances in (hetero)dimetallic systems towards tandem catalysis, Coord. Chem. Rev. 2021, 434, 213803.

26 J. Campos, Bimetallic cooperation across the periodic table, Nat. Rev. Chem. 2020, 4, 696–702.

27 R. Govindarajan, S. Deolka, J. R. Khusnutdinova, Heterometallic bond activation enabled by unsymmetrical ligand sca ff olds: bridging the opposites, Chem. Sci. 2022, 13, 14008-14031.

28 L. Biancalana, F. Marchetti, Aminocarbyne ligands in organometallic chemistry, Coord. Chem. Rev. 2021, 449, 214203.

29 G. Agonigi, M. Bortoluzzi, F. Marchetti, G. Pampaloni, S. Zacchini, V. Zanotti, Regioselective Nucleophilic Additions to Diiron Carbonyl Complexes Containing a Bridging Aminocarbyne Ligand: A Synthetic, Crystallographic and DFT Study, Eur. J. Inorg. Chem. 2018, 960–971.

30 G. Agonigi, L. Biancalana, M. G. Lupo, M. Montopoli, N. Ferri, S. Zacchini, F. Binacchi, T. Biver, B. Campanella, G. Pampaloni, V. Zanotti and F. Marchetti, Exploring the Anticancer Potential of Diiron Bis-cyclopentadienyl Complexes with Bridging Hydrocarbyl Ligands: Behavior in Aqueous Media and In Vitro Cytotoxicity, Organometallics 2020, 39, 645-657.

31 L. Biancalana, M. De Franco, G. Ciancaleoni, S. Zacchini, G. Pampaloni, V. Gandin, F. Marchetti, Easily Available and Amphiphilic Diiron Cyclopentadienyl Complexes Exhibit In Vitro Anticancer Activity in 2D and 3D Human Cancer Cells via Redox Modulation Triggered by CO Release. Chem. Eur. J. 2021, 27, 10169–10185

32 L. Biancalana, G. Ciancaleoni, S. Zacchini, G. Pampaloni, F. Marchetti, Carbonyl-isocyanide mono-substitution in $[Fe_2Cp_2(CO)_4]$: A re-visitation, Inorg. Chim. Acta 2020, 517, 120181.

33 Tolbatov, I.; Barresi, E.; Taliani, S.; La Mendola, D.; Marzo, T.; Marrone, A. Diruthenium(II,III) paddlewheel complexes: effects of bridging and axial ligands on anticancer properties, Inorg. Chem. Front., 2023, 10, 2226-2238

34 Rahman, F.-U.; Zeeshan Bhatti, M.; Ali, A.; Duong, H.-Q.; Zhang, Y.; Ji, X.; Lin, Y.; Wang, H.; Li, Z. T.; Zhang, D.-W. Dimetallic Ru(II) arene complexes appended on bis-salicylaldimine induce cancer cell death and suppress invasion via p53-dependent signaling, Eur. J. Med. Chem. 2018, 157, 1480-1490.

35 Wang, J.; Zhang, Y.; Li, Y.; Li, E.; Ye, W.; Pan, J. Dinuclear Organoruthenium Complex for Mitochondria-Targeted Near-Infrared Imaging and Anticancer Therapy to Overcome Platinum Resistance, Inorg. Chem. 2022, 61, 8267 – 8282.

36 D. Stíbal, B. Therrien, G. Süss-Fink, P. Nowak-Sliwinska, P. J. Dyson, E. Čermáková, M. Řezácová, P. Tomšík, Chlorambucil conjugates of dinuclear p-cymene ruthenium trithiolato complexes: synthesis, characterization and cytotoxicity study in vitro and in vivo, J Biol. Inorg. Chem. 2016, 21, 443–452.

37 A. A. Nazarov, M.-G. Mendoza-Ferri, M. Hanif, B. K. Keppler, P. J. Dyson, C. G. Hartinger, Understanding the interactions of diruthenium anticancer agents with amino acids, J. Biol. Inorg. Chem. 23, 2018, 1159–1164

38 B. Herry, L. K. Batchelor, B. Roufosse, D. Romano, J. Baumgartner, M. Borzova, T. Reifenstahl, T. Collins, A. Benamrane , J. Weggelaar, M. C. Correia, P. J. Dyson, B. Blom, Heterobimetallic Ru(μ-dppm)Fe and homobimetallic Ru(μ-dppm)Ru complexes as potential anti-cancer agents, J. Organomet. Chem. 901, 2019, 120934

39 M. Maroto-Díaz, B. T. Elie, P. Gómez-Sal, J. Pérez-Serrano, R. Gómez, M. Contel, F. Javier de la Mata, Synthesis and anticancer activity of carbosilane metallodendrimers based on arene ruthenium(ii) complexes, Dalton Trans. 45, 2016, 7049-7066

40 L. P. M. Green, T. R. Steel, M. Riisom, M. Hanif, T. Söhnel, S. M. F. Jamieson, L. J. Wright, J. D. Crowley, C. G. Hartinger, Synthetic Strategy Towards Heterodimetallic Half-Sandwich Complexes Based on a Symmetric Ditopic Ligand, Front. Chem. 9, 2021, 786367, DOI: 10.3389/fchem.2021.786367

41 G. Bresciani, J. Vančo, T. Funaioli, S. Zacchini, T. Malina, G. Pampaloni, Z. Dvořák, Z. Trávníček, F. Marchetti, Anticancer Potential of Diruthenium Complexes with Bridging Hydrocarbyl Ligands from Bioactive Alkynols, Inorg. Chem. 2023, 62, 15875–15890.

42 G. Bresciani, S. Boni, T. Funaioli, S. Zacchini, G. Pampaloni, N. Busto, T. Biver, F. Marchetti, Adding Diversity to a Diruthenium Biscyclopentadienyl Scaffold via Alkyne Incorporation: Synthesis and Biological Studies, Inorg. Chem. 2023, 62, 12453−12467.

43 J. A. S. Howell, A. J. Rowan, Synthesis and Fluxional Character of Complexes of the Type $[M_2(cp)_2(CO)_3(CNR)]$(M = Fe or Ru, Cp = η-C_5H_5), J. Chem. Soc. Dalton Trans. 1980, 503–510

44 L. Busetto, L. Carlucci, V. Zanotti, V.G. Albano, M. Monari, Ruthenium complexes with bridging functionalized alkylidene ligands. Synthesis of $[Ru_2Cp_2(CO)_2$(u-CO){u-C(X)N(Me)CH_2Ph}] (X = H, CN) and molecular structure of the CN derivative, J. Organomet. Chem. 1993, 447, 271-275.

45 V. G. Albano, L. Busetto, L. Carlucci, M. C. Cassani, M. Monari, V. Zanotti, Synthesis of dinuclear iron and ruthenium aminoalkylidene complexes and the molecular structure of the novel cis-$[Ru_2(CO)_2(Cp)_2${μ-C(CN)N(Me)Bz}$_2$](Cp = η-C_5H_5; Bz = CH_2Ph), J. Organomet. Chem. 1995, 488, 133-139.

46 L. Biancalana, M. Fiaschi, G. Ciancaleoni, G. Pampaloni, V. Zanotti, S. Zacchini, F. Marchetti, A comparative structural and spectroscopic study of diiron and diruthenium isocyanide and aminocarbyne complexes, Inorg. Chim. Acta 2022, 536, 120886.

47 L. Busetto, F. Marchetti, S. Zacchini, V. Zanotti, New diruthenium vinyliminium complexes from the insertion of alkynes into bridging aminocarbynes, J. Organomet. Chem. 2006, 691, 2424-2439,and references therein.

48 *General procedure*: a solution of $[Ru_2Cp_2(CO)_4]$ (150 mg, 0.30 mmol) and the selected isocyanide (2-naphthyl, benzyl, 4-methoxyphenyl, (diethoxyphosphoryl)methanyl, ((p-tolyloxy)sulfonyl)methanyl, (*S*)-2-phenylpropan-1-yl or 4-ethylphenyl isocyanide) in MeCN (15 mL) was stirred at room temperature for 24 h and then at reflux for 24 h while monitored by IR spectroscopy.

49 Compound $[Ru_2Cp_2(CO)_4]$ was also unreactive with benzyl isocyanide and 2-naphthyl isocyanide in refluxing THF (24 h).

50 IR (CH_2Cl_2): ϋ/cm^{-1} = 2056, 2003 cm^{-1}. T. Blackmore, J. D. Cotton, M. I. Bruce, F. G. A. Stone. Chemistry of the metal carbonyls. Part LIII. Some dicarbonyl-(π-cyclopentadienyl)ruthenium complexes containing metal–metal bonds. J. Chem. Soc. A, 1968, 2931-2936.

51 (a) A. R. Manning, G. McNally, D. Cunningham, P. McArdle, J. M. Simmi, The reactions of sulfuryl chloride with $[Fe_2(C_5H_5)_2(CO)_{4-n}(CNMe)_n]$ (n = 0,1,2 and 4) and related complexes. The crystal structure of $[Fe(C_9H_7)(CO)_3][FeCl_4]$, J. Organomet. Chem. 338, 1988, 383-392. (b) M. A. El-Hinnawi, M. L. Sumadi, F. T. Esmadi, I. Jibril, W. Imhof, G. Huttner, Organoruthenium sulfur complexes. Synthesis of (u-S_5)$[RuCp(CO)_2]_2$ and its reaction with acid chlorides. Preparation of $RuCp(CO)_2$(SCOR) and molecular structure of $RuCp(CO)_3SCO(2\text{-}O_2NC_6H_4)$, J. Organomet. Chem. 1989, 377, 373-381.

52 The spectroscopic characterization of impure [**2e-g**]CF_3SO_3 is limited to ^{1}H NMR ($CDCl_3$) and IR (CH_2Cl_2).

53 *Trans*-$[Fe_2Cp_2(CO)_2(\mu\text{-}CO)\{\mu\text{-}CN(R)(R')\}]^+$ complexes were identified (as minor isomers) only for R = R' = Me, Et. G. Cox, C. Dowling, A. R. Manning, P. McArdle, D. Cunningham, A reinvestigation of the reaction of $[Fe_2(\eta\text{-}C_5H_5)_2(CO)_{4-n}(CNR)_n]$ (n = 1 or 2) with strong alkylating agents. J. Organomet. Chem. 1992, 438, 143-158.

54 A. K. Hughes, K. Wade, Coord. Chem. Rev. 2000, 197, 191–229.

55 F. Basolo, Polyhedron 1990, 9, 1503-1535.

56 S. A. Decker, M. Klobukowski, J. Am. Chem. Soc. 1998, 120, 9342 – 9355.

57 G. Bresciani, S. Zacchini, G. Pampaloni, M. Bortoluzzi, F. Marchetti, Diiron Aminocarbyne Complexes with NCE^- Ligands (E = O, S, Se), Molecules 2023, 28, 3251.

58 (a) V. G. Albano, L. Busetto, C. Castellari, M. Monari, A. Palazzi, V. Zanotti, Electrophilically promoted cyanide abstraction in diiron cyano(amino) alkylidene complexes: molecular structure of $[Fe_2(CO)_2(\eta\text{-}C_5H_5)_2(\mu\text{-}CO)\{\mu\text{-}CN(CH_2)_4CH_2\}][(OC)_5WCNW(CO)_5]$, J. Chem. Soc. Dalton Trans. 1993, 3661-3666; (b) P. Bladon, M. Dekker, G. R. Knox, D. Willison, G. A. Jaffari, R. J. Doedens, K. W. Muir, Amination of complexed carbon monoxide by N-nitrosamines: syntheses and structures of iron carbonyl and nitrosyl complexes and applications to heterocyclic synthesis, Organometallics 1993, 12, 1725-1741.

59 The *cis*/*trans* ratio observed (^{1}H NMR) in acetone-d_6 or $CDCl_3$ solutions of [**2a-d**]CF_3SO_3 is representative of the overall composition of the sample, since the compounds are fully soluble in these conditions. Conversely, the *cis*/*trans* ratio in the saturated D_2O solutions is determined by the relative solubility of each isomer. Note that the isomerization process is not accessible at room temperature.

60 A. Leonidova, P. Anstaett, V. Pierroz, C. Mari, B. Spingler, S. Ferrari and G. Gasser, Induction of Cytotoxicity through Photorelease of Aminoferrocene, Inorg. Chem., 2015, 54, 9740 – 9748.

61 P. Marzenell, H. Hagen, L. Sellner, T. Zenz, R. Grinyte, V. Pavlov, S. Daum and A. Mokhir, Aminoferrocene-Based Prodrugs and Their E ff ects on Human Normal and Cancer Cells as Well as Bacterial Cells, J. Med. Chem., 2013, 56, 6935-6944.

62 A. C. Kautz, P. C. Kunz, C. Janiak, CO-releasing molecule (CORM) conjugate systems, Dalton Trans., 2016, 45 , 18045–18063.

63 The fraction of residual starting material after 72 h in deuterated water or water/methanol mixtures ranges from 50 to 90 %, depending on the *N*-substituents of the aminocarbyne ligand. See ref 31.

64 A. Boni, F. Marchetti, G. Pampaloni, S. Zacchini, Cationic Diiron and Diruthenium l-Allenyl Complexes: Synthesis, X-Ray Structures and Cyclization Reactions with Ethyldiazoacetate/Amine Affording Unprecedented Butenolide- and Furaniminium-Substituted Bridging Carbene Ligands, Dalton Trans., 2010, 39, 10866–10875.

65 G. Bresciani, S. Boni, S. Zacchini, G. Pampaloni, M. Bortoluzzi, F. Marchetti, Alkyne–alkenyl coupling at a diruthenium complex, Dalton Trans. 2022, 51, 15703-15715.

66 E. Van Caemelbecke, T. Phan, W. R. Osterloh, K. M. Kadish, Electrochemistry of metal-metal bonded diruthenium complexes, Coord. Chem. Rev. 2021, 434, 213706.

67 R. Mazzoni, A. Gabiccini, C. Cesari, V. Zanotti, I. Gualandi, D. Tonelli, Diiron complexes bearing bridging hydrocarbyl ligands as electrocatalysts for proton reduction, Organometallics 2015, 34, 3228–3235.

68 C. Saviozzi, L. Biancalana, T. Funaioli, M. Bortoluzzi, M. De Franco, M. Guelfi, V. Gandin, F. Marchetti, A Triiron Complex with N-Ferrocenyl Aminocarbyne Ligand Bridging a Diiron Core: DFT, Electrochemical and Biological Insights, Inorg. Chem. 2024, 63, 2, 1054–1067.

69 B. Callan, A. R. Manning, The reactions of AgI electrophile with $[Fe_2(\eta\text{-}C_5H_5)_2(CO)_2(L)\{CN(Me)H\}]^+$ and $[Fe_2(\eta\text{-}C_5H_5)_2(CO)_2\{CN(Me)H\}_2]^{2+}$ salts (L = CO or CNMe), J. Organomet. Chem. 1986, 316, 325-333.

70 (a) E. Reisner, V. B. Arion, M. F. C. Guedes da Silva, R. Lichtenecker, A. Eichinger, B. K. Keppler, V. Yu. Kukushkin,A. J. L. Pombeiro, Tuning of Redox Potentials for the Design of Ruthenium Anticancer Drugs - an Electrochemical Study of $[trans\text{-}RuCl_4L(DMSO)]^-$ and $[trans\text{-}RuCl_4L_2]^-$ Complexes, where L = Imidazole, 1,2,4-Triazole, Indazole, Inorg. Chem., 2004, 43, 7083–7093. (b) W. G. Kirlin, J. Cai, S. A. Thompson, D. Diaz, Glutathione Redox Potential in Response to Differentiation and Enzyme Inducers, Free Radical Biol. Med., 1999, 27, 1208–1218.

71 C. Scolaro, A. Bergamo, L. Brescacin, R. Delfino, M. Cocchietto, G. Laurenczy, T. J. Geldbach, G. Sava, P. J. Dyson, In Vitro and in Vivo Evaluation of Ruthenium(II)-Arene PTA Complexes, J. Med. Chem. 2005, 48, 4161-4171.

72 T. T. Fong, C. N. Lok, C. Y. Chung, Y. M. Fung, P. K. Chow, P. K. Wan, C. M. Che, Cyclometalated Palladium(II) N-Heterocyclic Carbene Complexes: Anticancer Agents for Potent In Vitro Cytotoxicity and In Vivo Tumor Growth Suppression, Angew. Chem. Int. Ed. 2016, 55, 11935-11939.

73 O. A. Lenis-Rojas, M. P. Robalo, A. I. Tomaz, A. Carvalho, A. R. Fernandes, F. Marques, M. Folgueira, J. Yáñez, D. Vázquez-García, M. López Torres, A. Fernández, J. J. Fernández, Half-Sandwich Iridium(III) and Ruthenium(II) Complexes Containing P^P-Chelating Ligands: A New Class of Potent Anticancer Agents with Unusual Redox Features, Inorg. Chem. 2018, 57, 13150-13166.

74 Y. Jia, X. Wen, Y. Gong, X. Wang, Current scenario of indole derivatives with potential anti-drug-resistant cancer activity, Eur. J. Med. Chem. 2020, 200, 112359.

75 Y. Wan, Y. Li, C. Yan, M. Yan, Z. Tang, Indole: a privileged scaffold for the design of anti-cancer agents, Eur. J. Med. Chem. 2019, 183, 111691.

76 S. Dadashpour, S. Emami, Indole in the target-based design of anticancer agents: a versatile scaffold with diverse mechanisms, Eur. J. Med. Chem. 2018, 150, 9-29.

77 G. Bresciani, J. Cervinka, H. Kostrhunova, L. Biancalana, M. Bortoluzzi, G. Pampaloni, V.Novohradsky, V. Brabec, F. Marchetti, J. Kasparkova, N-Indolyl diiron vinyliminium complexes exhibit antiproliferative effects in cancer cells associated with disruption of mitochondrial homeostasis, ROS scavenging, and antioxidant activity, Chemico-Biol. Int. 2023, 385, 110742.

78 N. Oberhuber, H. Ghosh, B. Nitzsche, P. Dandawate, M. H ¨ opfner, R. Schobert, B. Biersack, Synthesis and anticancer evaluation of new indole-based tyrphostin derivatives and their (p-cymene)dichloridoruthenium(II) complexes, Int. J. Mol. Sci. 2023, 24.

79 N. Nayeem, A.Yeasmin, S. N. Cobos, A. Younes, K. Hubbard, M. Contel, Investigation of the Effects and Mechanisms of Anticancer Action of a Ru(II)-Arene Iminophosphorane Compound in Triple Negative Breast Cancer Cells. ChemMedChem. 2021, 16, 3280-3292.

80 Z. Riaz, B. Y. T. Lee, J. Stjärnhage, S. Movassaghi, T. Söhnel, S. M. F. Jamieson, M. A. Shaheen, M. Hanif, C. G. Hartinger, Anticancer Ru and Os complexes of N-(4-chlorophenyl)pyridine-2-carbothioamide: Substitution of the labile chlorido ligand with phosphines. J. Inorg. Biochem. 2023, 241, 112115.

81 B. S. Murray, M. V. Babak, C. G. Hartinger, P. J. Dyson, The development of RAPTA compounds for the treatment of tumors. Coord. Chem. Rev. 2016, 306, 86−114.

82 V. Velma, S. R. Dasari, P. B. Tchounwou, Low Doses of Cisplatin Induce Gene Alterations, Cell Cycle Arrest, and Apoptosis in Human Promyelocytic Leukemia Cells. Biomark Insights 2016, 11, 113−121.

83 R. Chavez-Dominguez, M. Perez-Medina, J. S. Lopez-Gonzalez, M. Galicia-Velasco, D. Aguilar-Cazares, The Double-Edge Sword of Autophagy in Cancer: From Tumor Suppression to Pro-tumor Activity. Front. Oncol. 2020, 10:578418. doi: 10.3389/fonc.2020.578418.

84 G. Kroemer, G. Mariño, B. Levine, Autophagy and the integrated stress response. Mol Cell. 2010, 22, 280-293.

85 S. Dasari, P. B. Tchounwou, Cisplatin in cancer therapy: molecular mechanisms of action. Eur. J. Pharmacol. 2014, 740, 364−378.

86 E. Alessio, L. Messori, NAMI-A and KP1019/1339, Two Iconic Ruthenium Anticancer Drug Candidates Face-to-Face: A Case Story in Medicinal Inorganic Chemistry, Molecules 2019, 24, 1995.

87 S. Thota, D. A. Rodrigues, D. C. Crans, E. J. Barreiro, Ru(II) Compounds: Next-Generation Anticancer Metallotherapeutics?, J. Med. Chem. 2018, 61, 5805-5821.

88 R. E. Schuster, J. E. Scott, J. Casanova Jr., Methyl Isocyanide, Org. Synth. 46, 1966, 75.

89 (a) M. A. Mironov, M. I. Tokareva, M. N. Ivantsova, V. S. Mokrushin, Ugi Reaction with Isocyanoindoles, Russ. J. Org. Chem. 2004, 40, 847–853; (b) J. Yin, J. Zhang, C. Cai, G.-J. Deng, H. Gong, Catalyst-Free Transamidation of Aromatic Amines with Formamide Derivatives and Tertiary Amides with Aliphatic Amines, Org. Lett. 2019, 21, 387−392.

90 G. R. Fulmer, A. J. M. Miller, N. H. Sherden, H. E. Gottlieb, A. Nudelman, B. M. Stoltz, J. E. Bercaw and K. I. Goldberg, NMR Chemical Shifts of Trace Impurities: Common Laboratory Solvents, Organics, and Gases in Deuterated Solvents Relevant to the Organometallic Chemist. Organometallics, 2010, 29, 2176-2179.

91 R. K. Harris, E. D. Becker, S. M. Cabral De Menezes, R. Goodfellow and P. Granger, NMR nomenclature. Nuclear spin properties and conventions for chemical shifts (IUPAC Recommendations 2001). Pure Appl. Chem., 2001, 73, 1795-1818.

92 F. Menges, "Spectragryph - optical spectroscopy software", Version 1.2.16.1, @ 2016-2022, http://www.effemm2.de/spectragryph.

93 G. Albano, L. Busetto, M. Monari, V. Zanotti, Reactions of acetonitrile di-iron m-aminocarbyne complexes; synthesis and structure of [Fe2(μ-CNMe2)(m-H)(CO)2(Cp)2], J. Organomet. Chem. 2000, 606, 163-168.

94 Removal of released carbon monoxide from the Schlenk line (by vacuum/N_2 cycles) after 2-3 hours from the beginning of the reaction is beneficial for the CO/MeNC substitution.

95 A substantial drop in the isolated yield of the μ-aminocarbyne complex and a parallel increase in $\{CpRu^{II}(CO)_2\}^+$ by-products was observed when using a higher amount of methyl triflate. Note that, on considering the incomplete CO/isocyanide exchange in the first step, an excess of the methylating agent is present the reaction mixture even when CF_3SO_3Me is added in equimolar amount with respect to the starting material $[Ru_2Cp_2(CO)_4]$.

96 Compound [**2b**]CF_3SO_3 was isolated in 50 % yield when toluene was employed as solvent in the first step, otherwise following an identical procedure.

97 Small amounts of $[Ru_2Cp_2(CO)_2(CNXyl)_2]$ were always obtained, even when the reaction was performed with excess $[Ru_2Cp_2(CO)_4]$ (1.5 eq. *vs*. XylNC). Compounds **1c** and $[Ru_2Cp_2(CO)_2(CNXyl)_2]$ are best separated at this stage, taking advantage of their different solubility in MeCN. Otherwise, separation of $[\mathbf{2c}]^+$ from $[Ru_2Cp_2(CO)_2(CNXyl)\{\mu\text{-}CNMe(Xyl)\}]^+$ by alumina chromatography is tricky.

98 Attempts to isolate **1e-g** by alumina chromatography have not been successful.

99 G. M. Sheldrick, SADABS-2008/1 - Bruker AXS Area Detector Scaling and Absorption Correction, Bruker AXS: Madison, Wisconsin, USA, 2008.

100 G. M. Sheldrick, Crystal structure refinement with SHELXL. Acta Cryst. C 2015, 71, 3.

101 (a) OECD Guidelines for Testing of Chemicals. In OECD, Paris: 1995; Vol. 107; (b) J. C. Dearden, G. M. Bresnen, The Measurement of Partition Coefficients, Quant. Struct.-Act. Relat. 1988, 7, 133-144.

102 Methanol was used as a co-solvent to prepare solutions suitable for ^1H NMR analysis (> 3 mM); the methanol/water ratio was selected with respect to the water solubility of the compound.

103 Calculated by the formula pD = pH* + 0.4, where pH* is the value measured for H_2O-calibrated pH-meter; (a) C. C. Westcott, pH Measurements; Academic Press: New York, 1978; (b) A. K. Covington, M. Paabo, R. A. Robinson and R. G. Bates. Anal. Chem. 1968, 40, 700-706.

104 M. Gross, J. Jordan, Voltammetry at Glassy Carbon Electrodes, Pure Appl. Chem. 1984, 56, 1095-1129.